CONTRACTOR REPORT

SAND85-8177
UC-62d
Unlimited Release

Theory of Cellwise Optimization for Solar Central Receiver Systems

University of Houston

Prepared by Sandia National Laboratories, Albuquerque, New Mexico 87185 and Livermore, California 94550 for the United States Department of Energy under Contract DE-AC04-76DP00789.

Printed May 1985

Printed in the United States of America
Available from
National Technical Information Service
5285 Port Royal Road
Springfield, VA 22161

NTIS price codes
Printed copy: A05
Microfiche copy: A01

UC-62d

SAND 85-8177
Unlimited Release
Printed May 1985

THEORY OF CELLWISE OPTIMIZATION FOR SOLAR CENTRAL RECEIVER SYSTEMS

F. W. Lipps
Energy Laboratory
University of Houston
4800 Calhoun Street
Houston, Texas 77004
September 1, 1981

Prepared with support of
U.S. Department of Energy
Under Contract SNLL-84-1637

FOREWORD

The research and development described in this report was conducted within the U.S. Department of Energy's (DOE) Solar Thermal Technology Program. The Solar Thermal Technology Program directs efforts to advance solar thermal technologies through research and development of solar thermal materials, components, and subsystems, and through testing and evaluation of solar thermal systems. These efforts are carried out through DOE and its network of national laboratories who work with private industry. Together they have established a goal-directed program for providing technically proven and economically competitve options for incorporation into the Nation's energy supply.

There are two primary solar thermal technologies: central receivers and distributed receivers. These two technologies use various point and line-focus optics to concentrate sunlight onto receivers where the solar energy is absorbed as heat and converted to electricity or used as process heat. In central receiver systems, which this report considers, fields of heliostats (two-axis tracking mirrors) focus sunlight onto a single receiver mounted on a tower. The radiant energy is absorbed by a working fluid circulating within the receiver and is transformed into high temperature thermal energy. Temperatures in central receivers may exceed $1500^{o}C$.

September 1981

SAN/1637-1

Theory of Cellwise Optimization for Solar Central Receiver Systems

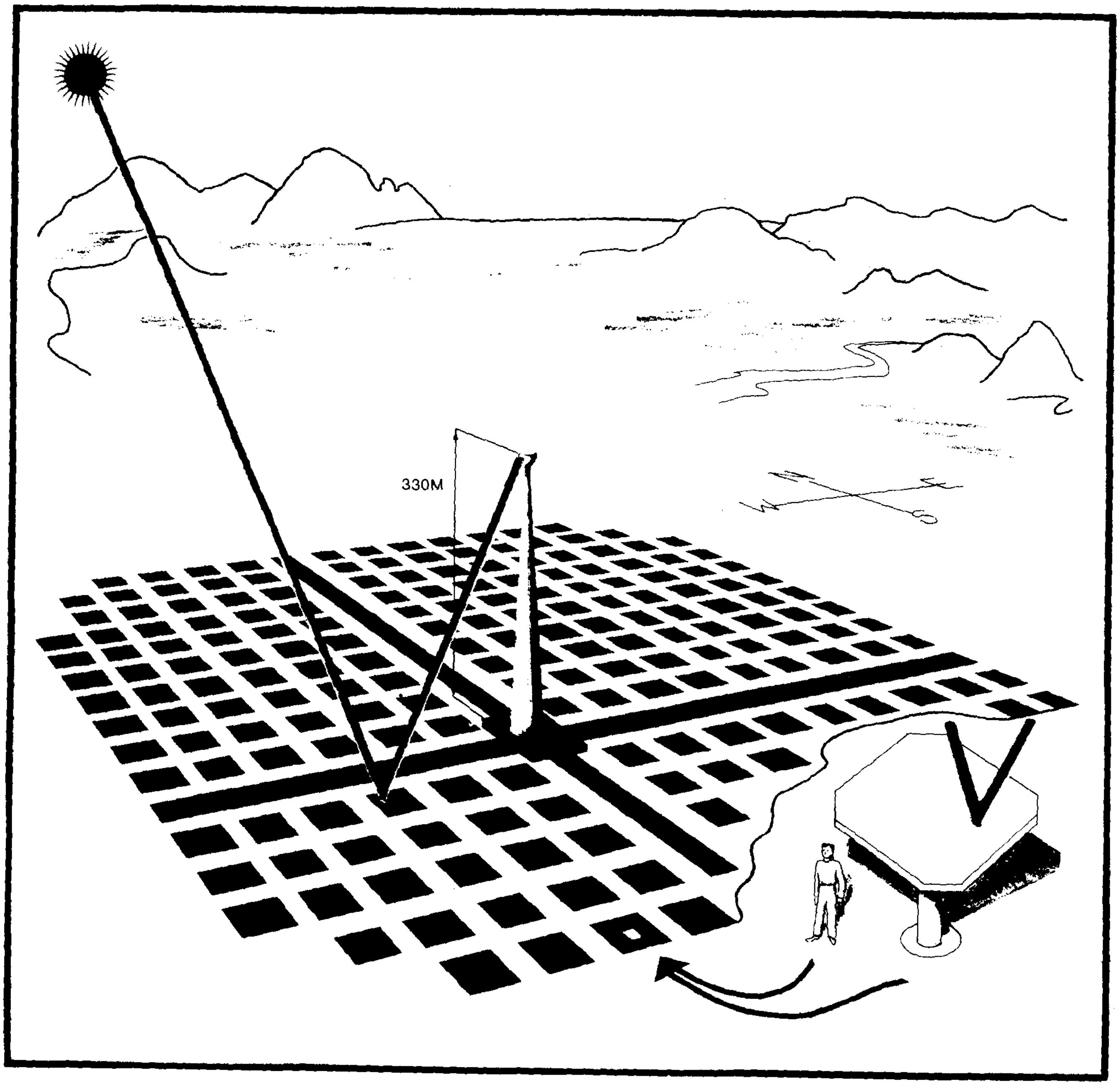

A Code Documentation Project
prepared by the
Solar Thermal Division
Energy Laboratory, University of Houston

University of Houston
Houston, Texas 77004

Prepared for the
U.S. Department of Energy
Solar Energy Div.
Under SNLL Contract 84-1637

Solar Energy System Simulation
and Analysis for Central Receiver
Systems

7/8

Abstract

Cost effective optimization of the solar central receiver system is primarily concerned with the distribution of heliostats in the collector field, including the boundaries of the field. The cellwise optimization procedure determines the optimum cell usage and heliostat spacing parameters for each cell in the collector field. Spacing parameters determine the heliostat density and neighborhood structure uniformly in each cell. Consequently, the cellwise approach ignores heliostat mismatch at cell boundaries. Ignoring the cell boundary problem permits an easy solution for the optimum in terms of appropriately defined annual average data. Insolation, receiver interception, shading and blocking, cosine effects, and the cost parameters combine to control the optimum. Many trade-offs are represented. Outputs include the receiver flux density distribution for design time, coefficients for an actual layout, the optimum boundary and various performance and cost estimates for the optimum field.

It is also possible to optimize receiver size and tower height by a repeated application of the field optimization procedure.

Acknowledgement

This document was prepared with Department of Energy support under Sandia National Laboratories, Livermore, contract 84-1637. Optimization theory and code development is due to L. L. Vant-Hull, F. W. Lipps and M. D. Walzel. Prof. E. Rothman's editorial assistance is deeply appreciated.

TABLE OF CONTENTS

List of Figures

Nomenclature

a = Multiplicative loss factor including receiver absorbtivity

a_c = Coefficient for ground coverage (i.e. $f_c = a_c / R_c Z_c$)

A_c = Area of land in cell c (m^2)

A_H = Area of glass/heliostat (m^2)

A_G = Total area of glass in collector (m^2)

$\bar{A}$ = Area of land/cell in collector (m^2)

b = Subtractive loss constant including receiver radiation, conduction, and convection losses (MWH/yr)

$B, \bar{B}$ = Set of interior (exterior) cells in collector

B_c = Boundary ratio ($B_c = 1$ at boundary)

c = Cell index for collector field

C = Total cost of thermal subsystem to base of tower including feedwater pump but excluding thermal storage ($)

C_o = Fixed cost parameter ($)

C_h = Cost of heliostats/area ($/$m^2$)

$C_p(P)$ = Power dependent cost function ($)

D_H = Width of heliostat (m)

D_M = Mechanical limit (in units of D_H), i.e. diameter of clearout circle for heliostats

E = Total thermal energy available at the base of the tower (MWH/yr)

E_c = Re-directed energy/yr from cell c

f, f_c = Ground coverage fraction (cell c)

F = Figure of merit ($/annual MWH thermal at base of tower)

F^* = Shifted figure of merit for case of power dependent costs

h = Height of cylindrical receiver in meters (i.e. top to bottom)

$\bar{h}$ = Maximum height of receiver in meters

H = Set of useful hours in year

H_o = Estimated number of hours such that $E=H_oP_o$

$\bar{H}$ = Total hours/yr of useful daylight

p = Index for receiver mode heights (=1 ... Q)

$P(\tau)$ = Total thermal power at time τ

P_o = Total thermal power at design time

q = Index for receiver mode azimuths (=1 ... P)

r = Radius of cylindrical receiver (m)

$\bar{r}$ = Maximum radius of receiver (m)

R, R_c = Radial spacing parameters (cell c) in units of D_H

$R(\rho,Z)$ = Radial layout function of (ρ,Z)

$\hat{R}(\rho_c,Z_i)$ = Optimum radial spacing parameter for $\rho=\rho_c$ and $Z=Z_i$

$\bar{S}$ = Total annual direct beam insolation for the useful daylight hours (annual MWH/m^2)

T = Focal height of tower, i.e. height of center of receiver above plane of heliostat centers

V = Set of independent variables

Z, Z_c = Azimuthal spacing parameter (cell c) in units of D_H

α = Relative cost of land

$\beta_{1,2,3}$ = Relative cost of wiring for 3 kinds of wiring

δ = Prefix denoting "variation of"

δ_o = Input scale parameter for variations

∂_x = Partial derivative with respect to x

$\Delta\phi$ = Azimuthal angle separating heliostats in a circular layout

η_c = Receiver interception fraction for cell c

θ = Solar elevation angle (degrees)

θ_s = Solar elevation angle at start-up and shut-down (degrees)

Λ = Dimensionless total thermal energy for constrained optima

Γ = Cost function for constrained optima

λ_c = Dimensionless measure of energy redirected by cell c (i.e. $\lambda_c \equiv E_c/(\bar{S}A_c)$)

$\tilde{\mu}$ = Cell matching parameter (annual MWH/m^2)

ξ_c = Efficiency of heliostats for re-directing power from cell c

ρ_c = Radial distance to cell c (m)

ρ_n = Radial distance to circle n (m)

$\Sigma(\chi)$ = Proportional to $\partial_\chi F$ for mechanical constraint

$\sigma(\tau)$ = Direct beam insolation as function of time (W/m^2)

σ_o = Direct beam insolation at design time (W/m^2)

σ_s = Direct beam insolation at start-up and shut-down

τ = Time parameter (hours from local noon)

τ_o = Time of choice for design specifications (hours from local noon)

ϕ_c = Cell use fraction for cell c

χ = Angle in (R,Z) plane

ψ_c = Effective ground coverage fraction including land and wiring parameters

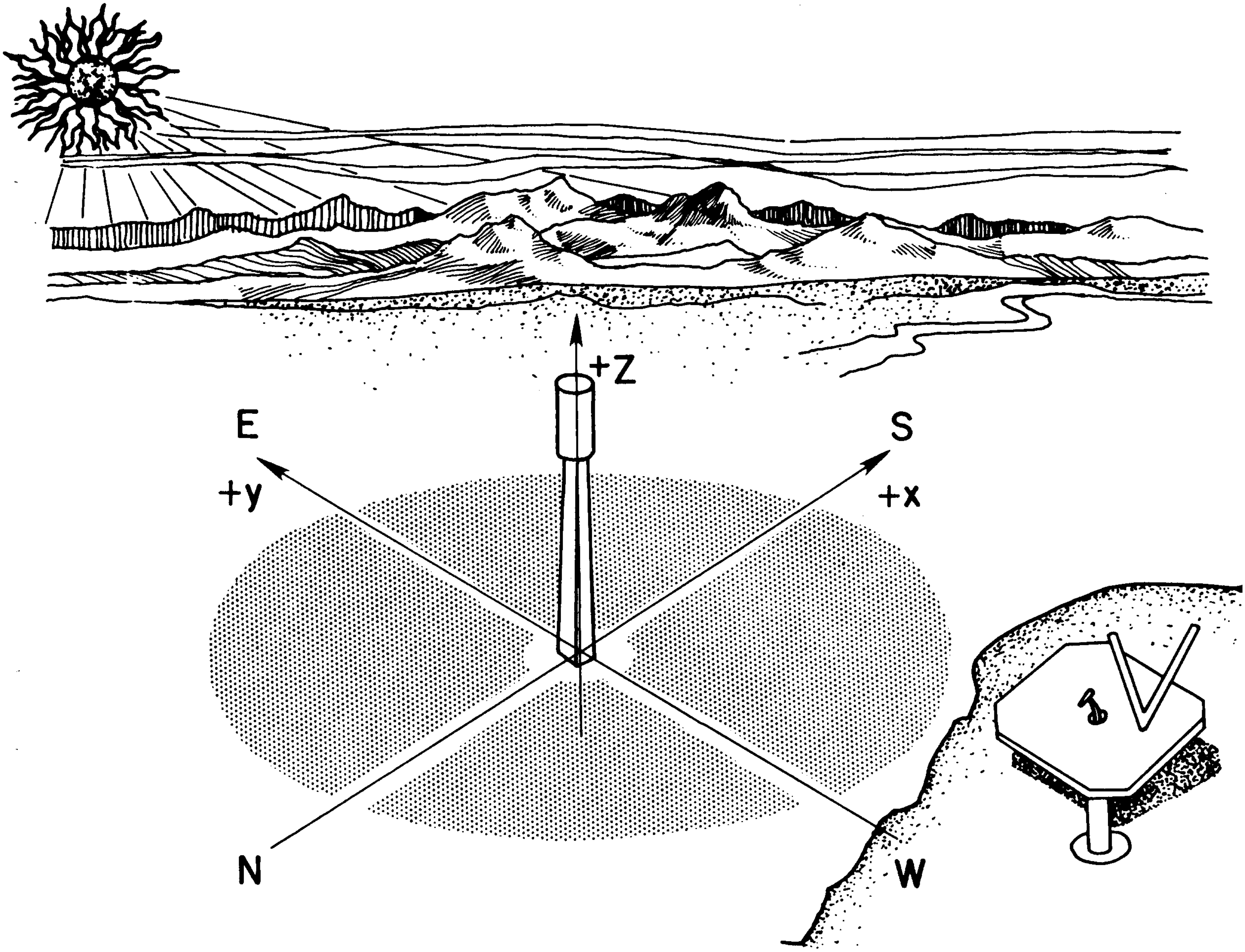

Figure 1.1 Artist's Concept of Central Receiver System.

Artist's Concept shows tower top receiver and collector field (shaded area). A typical heliostat is shown in lower right. In this case the receiver is cylindrical. The heliostats are individually guided to reflect sunlight on the central receiver. The optical system is a multi-segmented single surface reflection.

1. Introduction

The solar central receiver project at the University of Houston began in June of 1973 under an NSF/RANN grant. The UH System Analysis Group has been actively developing the optical analysis of the central receiver system from this time to the present (References 1 to 20). Figure 1.1 illustrates the system concept.

The central receiver system is a means of collecting high quality solar energy by optical transmission from a field containing a large number of independently guided and mass produced heliostats. Image resolution is not expected, but optical concentration is required in order to achieve an efficient energy transfer to the working fluid in the receiver. The complex geometry of the collector field and the large number of heliostats suggest the use of a cell model with a statistical assumption for the effect of guidance errors on the groups of heliostats belonging to individual cells.

An average year is defined by an average insolation model with monthly average weather parameters for cloud cover, turbidity, water vapor, and horizontal visibility. The thermal sub-system includes the collector field, tower, receiver, tower plumbing, and main feed pump, but not the thermal storage, turbine, or electric power generators.

More than half of the thermal sub-system cost is due to the collector, and therefore, the optimization is primarily concerned with the arrangement of heliostats in the collector field and the determination of its boundary. The optimum collector field geometry will be a state of minimum figure of merit. Generally, this implies that

$$\delta F = 0,$$

for all variations, but in section 4 an endpoint case occurs.

Complex geometries frequently lead to Monte Carlo simulation. Monte Carlo simulation is a statistical method for evaluating the performance of a given design, but it requires considerable CPU time and cannot be adapted to optimization. A cell model of the collector field provides an alternative approach to system simulation, which can also be used for optimization.

Details of the cell-wise performance model are contained in References 2 and 9. The theory of the cellwise optimization requires a few variables taken from the performance model. See section 2.

The economic optimization is based on a figure of merit

$$F = C/E,$$

where C is the total cost of the thermal subsystem and E is the total thermal energy collected in an average year. E is the energy produced at the base of the tower. Similarly, C is the cost of the thermal subsystem down to the base of the tower and not including thermal storage, or turbine generator, etc.

2. Cellwise Optimization Method

The total thermal energy collected in an average year can be expressed in terms of the cell model as follows.

$$E = a\bar{A}\bar{S}(\sum_c \eta_c \lambda_c f_c \phi_c) - b,$$

where

E	=	Total thermal energy available at the base of the tower,
a	=	Multiplicative loss factor including receiver absorbtivity,
b	=	Subtractive loss constant including receiver radiation, conduction, and convection losses,
c	=	Index of cells in collector field (See Figure 2.1),
$\bar{A}$	=	Area of land/cell in collector,
η_c	=	Receiver interception fraction for cell c,
λ_c	=	Dimensionless measure of energy redirected by cell c,
f_c	=	Ground coverage fraction for cell c,
ϕ_c	=	Cell use fraction for cell c, and
$\bar{S}$	=	$\int_H d\tau\sigma(\tau)$.

$\bar{S}$ is the total annual direct beam insolation for the useful hours of daylight. $\sigma(\tau)$ is the instantaneous direct beam insolation. The useful daylight is defined by the requirement

$$\sigma(\tau) \geq \sigma_s \text{ or } \theta \geq \theta_s,$$

where θ is the solar elevation angle. θ_s is the elevation of the sun at start-up or shut-down, and σ_s is the coresponding insolation. In practice θ_s is between 10° and 15°.

The total area of glass in cell c is given by

$$A_c = \bar{A}f_c\phi_c,$$

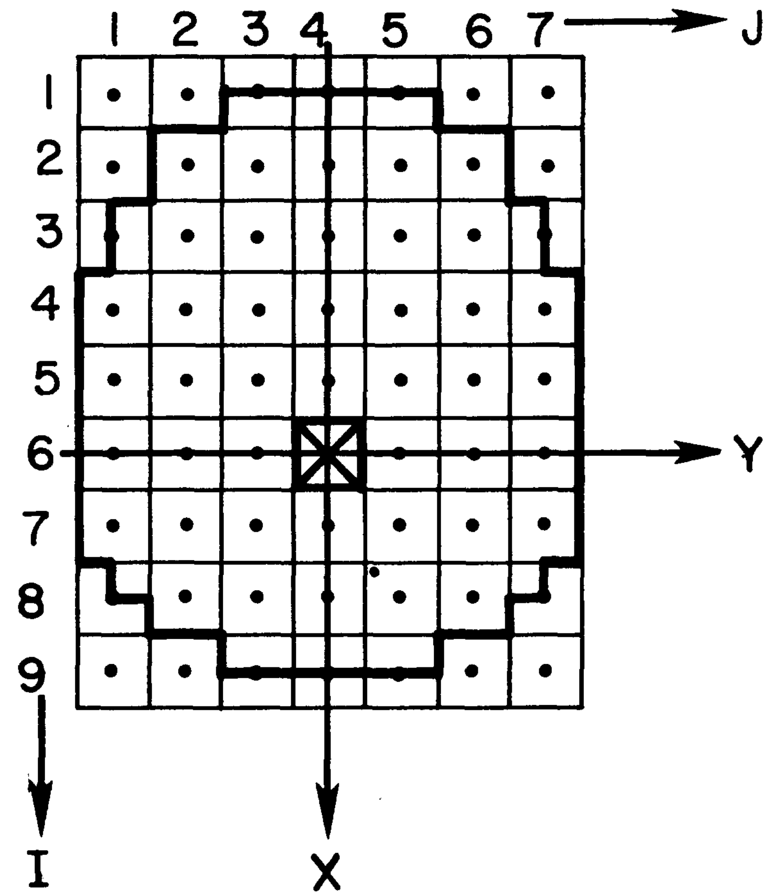

Figure 2.1 Cell Model of Collector Field.

The X axis points south and the Y axis points east. Heavy lines mark the outer boundary of the collector field. In this example the tower is located at cell (6,4), and only the tower cell is excluded by the inner boundary.

and the total area of glass in the collector is

$$A_G = \sum_c A_c = \bar{A}\sum_c f_c \phi_c .$$

The ground coverage fraction is given by (See Figure 2.2)

$$f_c = a_c/(R_c Z_c)$$

where

$$a_c = \begin{cases} 2A_H/D_H^2 & \text{for stagger neighborhoods,} \\ A_H/D_H^2 & \text{for cornfield neighborhoods,} \end{cases}$$

D_H = Width of heliostat,

A_H = Area of glass/heliostat (See Figure 2.3),

R_c = Radial spacing parameter for heliostat neighborhoods, and

Z_c = Azimuthal spacing parameter for heliostat neighborhoods. (See Figures 2.4 and 2.5).

R_c and Z_c are dimensionless multiples of D_H and must exceed unity because of the free-turning requirement. The so-called mechanical limits will be discussed as constraints in section 5.

The cellwise performance model defines the energy E_c which is re-directed towards the receiver by cell c. Details of this construction are not relevant to the optimization. However, the optimization theory is written in terms of the dimensionless quantity

$$\lambda_c(R_c,Z_c) = E_c(\bar{S}A_c).$$

λ_c is the ratio of redirected energy from cell C to the maximum total annual direct insolation available from cell C. λ_c depends on the location of cell c and the arrangement of neighbors via (R_c,Z_c).

The optimization determines the following set of independent variables:

$$V = \{(R_c,\ Z_c,\ \phi_c) \mid c = \text{cell index}\}.$$

ϕ_c is the dimensionless fraction of cell usage for cell c. ϕ_c=0 if the cell is

FRACTION OF GROUND COVERED UNIVERSITY OF HOUSTON

MAX(A) = 3.5261E-01 MIN(A) = 8.3149E-02 AVR(A) = 1.8803E-01

AIJ = (10 ** 0) X PRINTED VALUES

0.083	0.093	0.101	0.104	0.101	0.093	0.083	1.000
0.098	0.115	0.131	0.138	0.131	0.115	0.098	1.000
0.115	0.146	0.183	0.203	0.183	0.146	0.115	1.000
0.131	0.183	0.274	0.353	0.274	0.183	0.131	1.000
0.138	0.203	0.353	0.	0.353	0.203	0.138	1.000
0.131	0.183	0.274	0.353	0.274	0.183	0.131	1.000
0.115	0.146	0.183	0.203	0.183	0.146	0.115	1.000
0.098	0.115	0.131	0.138	0.131	0.115	0.098	1.000
1.000	1.000	1.000	1.000	1.000	1.000	1.000	0.188

Figure 2.2 Fraction of Ground Coverage Matrix.

The tower is located at cell (5,4). In this case the ground coverage fraction is independent of azimuth measured from the base of the tower. In general, this is not an exact symmetry for cellwise optimization. The bottom row and the right column represent averages of the corresponding rows and columns. The value in the lower right corner is the over-all average. In general, the array averages are glass weighted and for the average fraction of ground covered by glass is always 1.000. However the over-all average is land weighted for this array only.

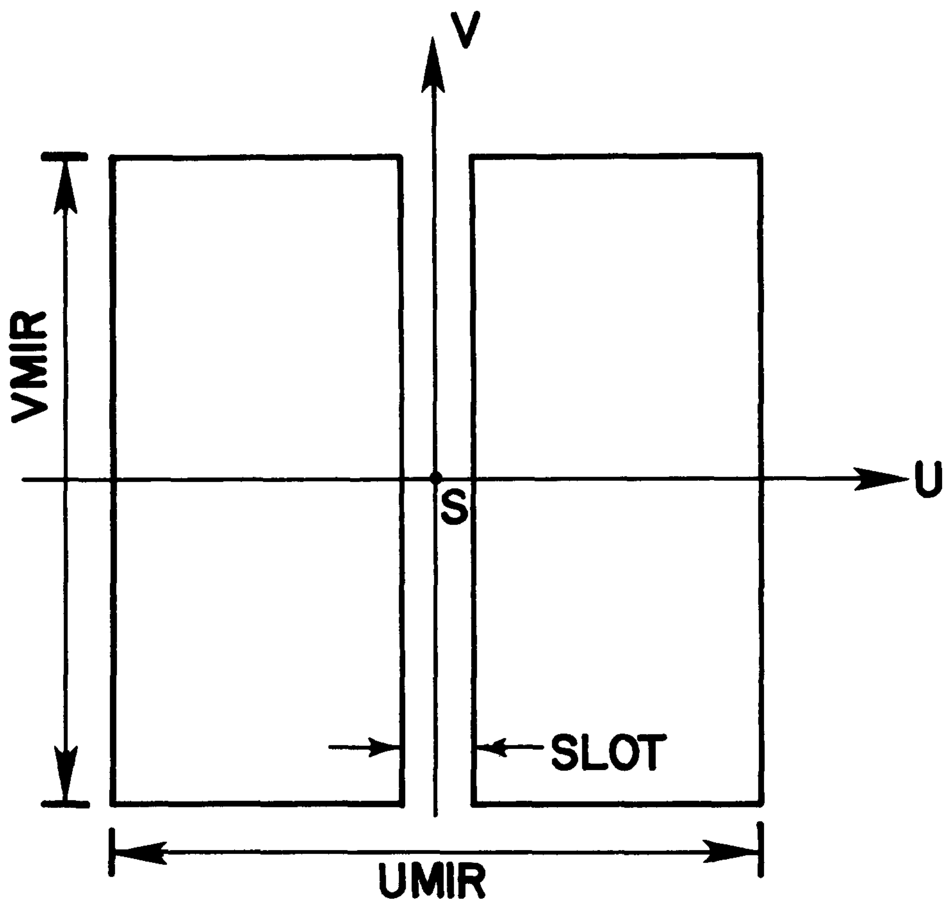

Figure 2.3 Rectangular Heliostat Geometry.

The U axis is horizontal in the usual altitude-azimuthal mounting system. A sun sensor can be located at S. The area of glass for shading and blocking calculations is

$$A_H = (UMIR-SLOT) * VMIR.$$

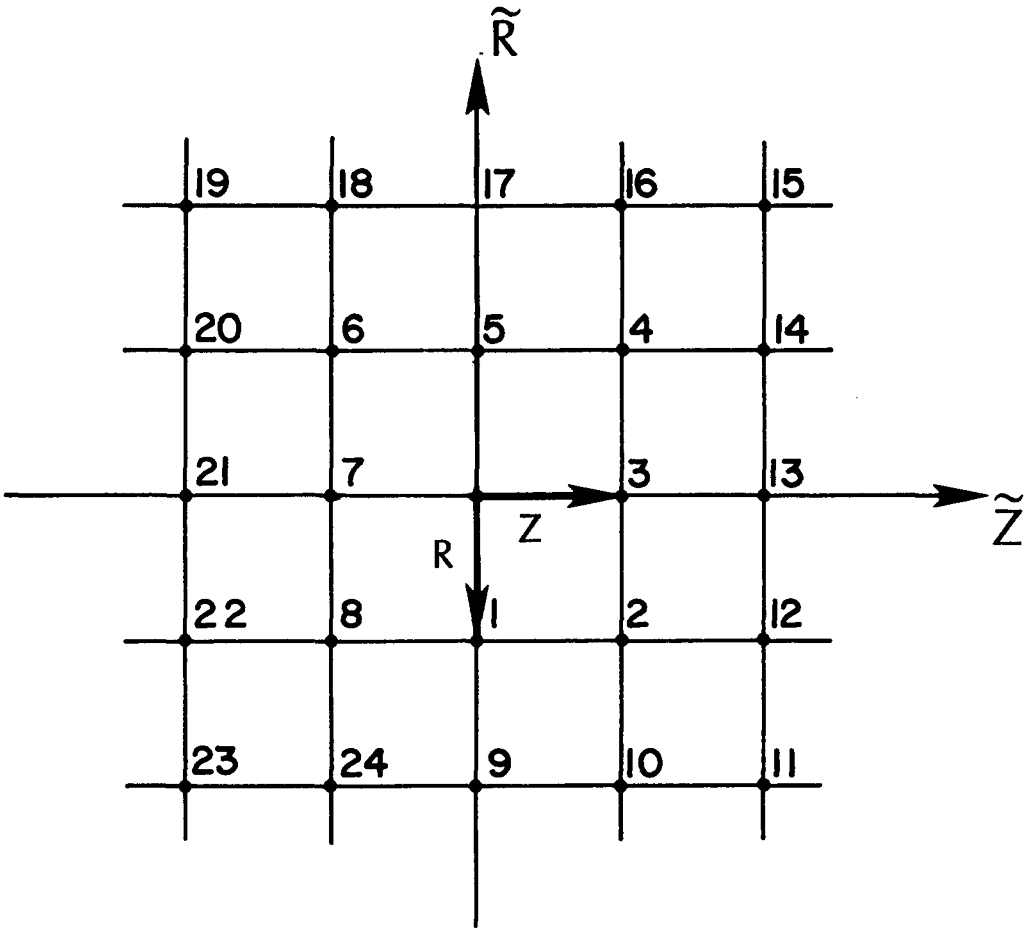

Figure 2.4 A Cornfield Type of Heliostat Neighborhood.

The R and Z spacing parameters are shown. Each neighbor is numbered as in the code. This figure shows first and second order neighbors.

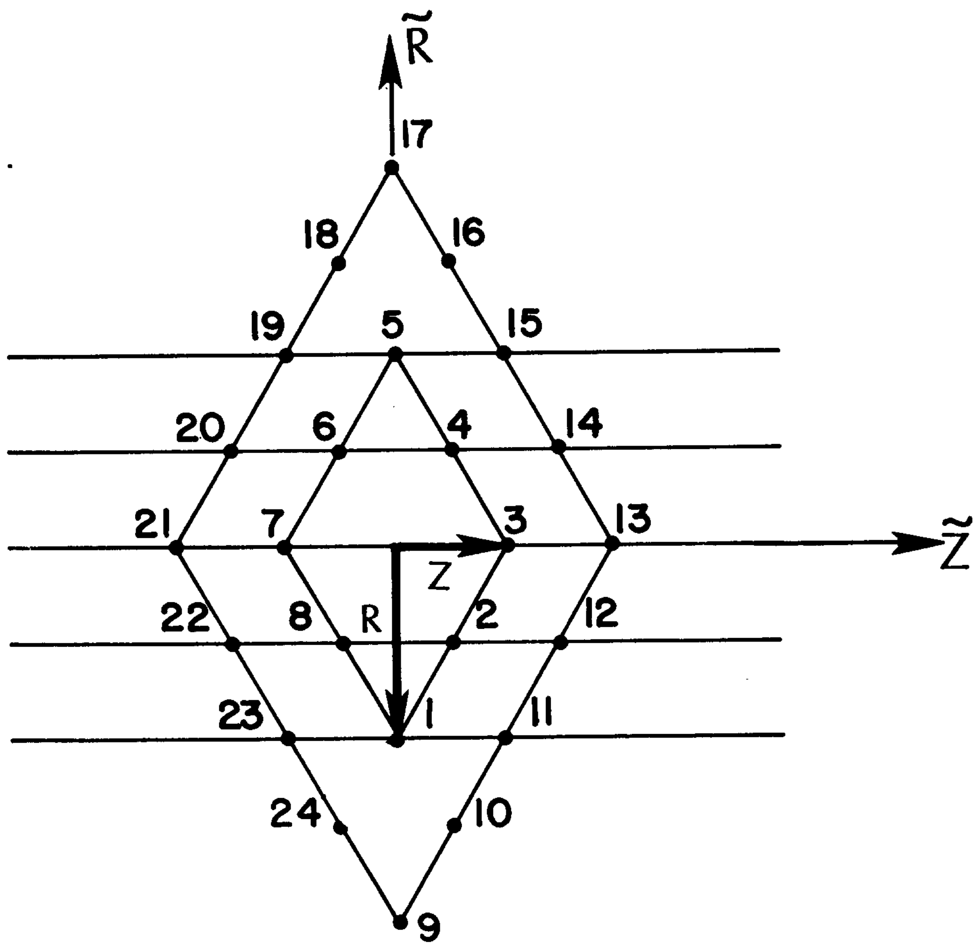

Figure 2.5 A Stagger Type of Heliostat Neighborhood.

The R and Z spacing parameters are shown. The horizontal lines represent tower concentric circles if the layout is radial stagger. Each neighbor is numbered as in the code. In radial stagger, neighbor #1 is towards the tower.

outside of the economically useful portion of the collector field, and $\phi_c=1$ if the cell is entirely inside of the useful region. $0<\phi_c<1$ for boundary cells. The optimized collector field has an inner and an outer boundary defined in terms of the set $\{\phi_c\}$.

2.1 Simple Cost Model

The simplest possible cost model includes a fixed cost C_o and a cost which is proportional to the total area of glass in the heliostat field A_G. In this case

$$C = C_o + C_h A_G.$$

This cost model assumes that land cost is either ignored or included in the fixed cost. Wiring cost is ~4% of $C_h A_G$ and is simply ignored.

$$A_G = \bar{A} \sum_c f_c \phi_c.$$

The optimization process requires known values for a, b, $\bar{S}$, $\bar{A}$, C_o, C_h, η_c, and $\lambda_c(R_c,Z_c)$.

We consider variations of the figure of merit, F, with respect to each of the variables in the set V. Assuming that the optimum occurs within the allowed range of all the variables,

$$\delta F = \delta(C/E) = (1/E)\delta C - (C/E^2)\delta E = 0$$

so that

$$F = C/E = \delta C/\delta E$$

for all choices of δ at the optimum point. In this simple case

$$\partial_{\phi_c} C = C_h f_c \bar{A}$$

$$\partial_{R_c} C = -C_h f_c \phi_c \bar{A}/R_c$$

$$\partial_{Z_c} C = -C_h f_c \phi_c \bar{A}/Z_c$$

$$\partial_{\phi_c} E = a\eta_c \lambda_c f_c \bar{S}\bar{A}$$

$$\partial_{R_c} E = a\eta_c(\partial_{R_c}\lambda_c - \lambda_c/R_c) f_c \phi_c \bar{S}\bar{A}$$

$$\partial_{Z_c} E = a\eta_c(\partial_{Z_c}\lambda_c - \lambda_c/Z_c) f_c \phi_c \bar{S}\bar{A}$$

The trim variable ϕ_c is limited to the range $0 \leqq \phi_c \leqq 1$. $\phi_c = 0$ if cell c is outside of the optimum field and $\phi_c = 1$ if cell c is inside of the optimum field. However, $0 < \phi_c < 1$ if the cell c is a boundary cell. For boundary cells, $\delta = \delta\phi_c\partial\phi_c$, gives

$$F = (\partial_{\phi_c} C)/(\partial_{\phi_c} E)$$

$$= C_h/(a\eta_c\lambda_c\bar{S})$$

so that

$$\eta_c\lambda_c = C_h/(Fa\bar{S}),$$

which can be satisfied approximately by the subset of cells called boundary cells. The exterior cells are discarded.

The stationary conditions for interior cells can be written as

$$\partial_{R_c} E = (\partial_{R_c} C)/F$$

and

$$\partial_{Z_c} E = (\partial_{Z_c} C)/F.$$

However, it is convenient to introduce an alternative parametrization of the neighborhood geometry. Let

$$f \equiv a_c/RZ$$

and

$$t \equiv 1/2\ (R^2 - Z^2)$$

so that

$$\lambda_c(R,Z) = \lambda_c(f,t).$$

It can be shown that

$$\partial f/\partial t = 0 = \partial t/\partial f$$

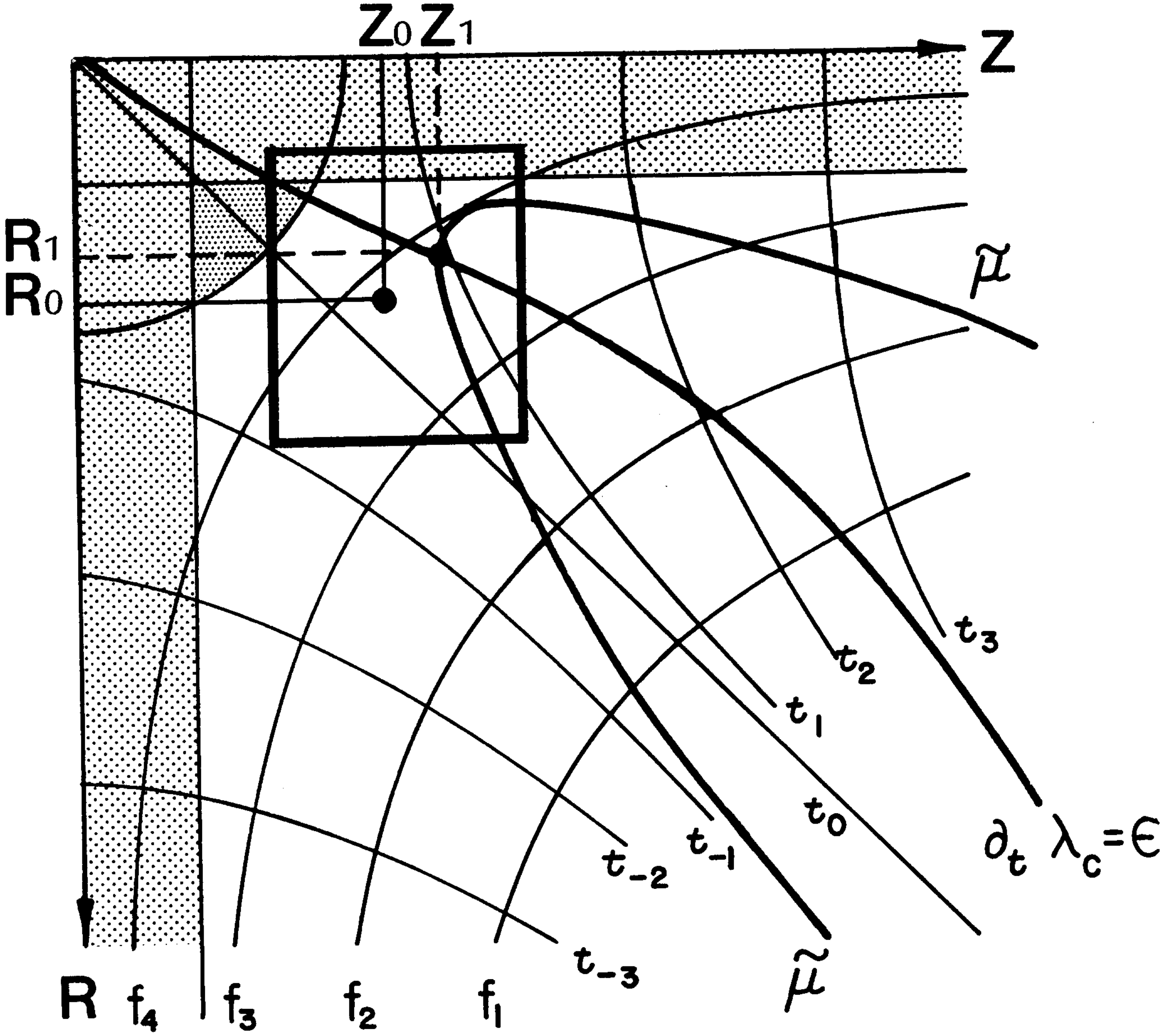

Figure 2.6 Alternative Parametrization of the Neighborhood Geometry.

Rectangular hyperbolas of constant f and t fill a quadrant of (R,Z) plane. (R_0,Z_0) is input estimate and (R_1,Z_1) is output optimum. The box around (R_0,Z_0) is the zone of variations. Heavy lines labeled $\tilde{\mu}$ and $\partial_{t_c} \lambda_c = \varepsilon$ define the optimum and represent theoretical optimum conditions. The shaded region represents mechanical limits.

so that curves of constant f and t are mutually orthogonal hyperbolas. See Figure 2.6. Consequently, the stationary conditions can be re-written as

$$\partial_{f_c} E = (\partial_{f_c} C)/F$$

and

$$\partial_{t_c} E = (\partial_{t_c} C)/F.$$

For interior cells we have $\phi_c \equiv 1$ so that

$$\partial_{t_c} C = 0 \qquad \text{(helpful!)}$$

$$\partial_{t_c} E = a\eta_c(\partial_{t_c} \lambda_c) f_c \bar{S}\bar{A}$$

$$\partial_{f_c} C = C_h \bar{A}$$

and

$$\partial_{f_c} E = a\eta_c(f_c \partial_{f_c} \lambda_c + \lambda_c)\bar{S}\bar{A} \ .$$

Consequently, the optimum geometry for an interior cell is determined by the two requirements

$$\partial_{t_c} \lambda_c = 0,$$

and

$$(f_c \partial_{f_c} \lambda_c + \lambda_c)\eta_c = \tilde{\mu} \equiv C_h/(Fa\bar{S}).$$

$\tilde{\mu}$ is called the cell matching parameter because it is independent of c. $\tilde{\mu}$ must be available to the optimizer. Note that $\tilde{\mu}$ depends on the figure of merit, F, which is estimated before the optimum can be determined, so that the whole solution process must be repeated to converge F(input) to F(output). Fortunately, convergence is quite rapid.

The cell matching parameter can be understood as follows.

$$\tilde{\mu} = C_h/(Fa\bar{S})$$
$$= C_h A_G E/(Ca\bar{S}A_G)$$
$$= (C_h A_G/C)(E/(a\bar{S}A_G))$$

Hence $\tilde{\mu}$ is the fraction of total cost due to heliostats times the fraction of available energy incident on the heliostats which is produced at the base of the tower.

The stationary condition for boundary cells gives

$$\partial_{\phi_c} E = (\partial_{\phi_c} C)/F,$$

or

$$a\eta_{c\lambda_c} f_c \bar{S}\bar{A} = C_h f_c \bar{A}$$

Consequently, if

$$B_c \equiv \eta_c \lambda_c / \tilde{\mu},$$

then $B_c = 1$ for boundary cells. B_c is always positive, but $B_c \to o$ as $\eta_c \to o$ for remote cells. Remote cells are external to the collector field and, hence by continuity, we conclude that

$$B_c < 1 \text{ for external cells, and}$$
$$B_c \geq 1 \text{ for internal cells.}$$

See Figure 2.7. Small η_c occurs if the cell has a large slant range or a poor receiver incidence angle (e.g., cylindrical receiver where the cell is too near the tower). Even if η_c is unity B_c may be less than one if the energy production λ_c is low either because of poor heliostat cosine factor (far to the south) or because of excessive shading and blocking. Hence, the inequality $B_c \geq 1$ trims the collector field and provides both the outer and inner boundary.

INTERCEPTION FACTORS FROM (CYLN) RECEIVER PROGRAM * * * * * UNIVERSITY OF

MAX(A) = 1.0017E 00 MIN(A) = 3.6247E-01 AVR(A) = 8.3409E-01

AIJ = (10 ** 0) X PRINTED VALUES

0.362	0.425	0.474	0.492	0.474	0.425	0.362	0.483
0.457	0.559	0.642	0.674	0.642	0.559	0.457	0.625
0.561	0.712	0.833	0.877	0.833	0.712	0.561	0.787
0.646	0.838	0.966	0.996	0.966	0.838	0.646	0.887
0.682	0.887	0.997	0.	0.997	0.887	0.682	0.902
0.651	0.847	0.974	1.002	0.974	0.847	0.651	0.894
0.567	0.723	0.850	0.895	0.850	0.723	0.567	0.850
0.462	0.568	0.654	0.688	0.654	0.568	0.462	0.672
0.653	0.796	0.887	0.874	0.887	0.796	0.653	0.834

Figure 2.7 Receiver Interception Matrix.

The tower is located at cell (5,4). The cylindrical receiver gives interception which is approximately independent of azimuth. Lack of symmetry is due to north-south asymmetry in orientation of heliostats. Cell size is too large to show reduced interception for near tower cells.

2.2 Complete Cost Model

A similar derivation can be given for other cost models. In practice, it is necessary to consider the cost of land and wiring. Let

$$C = C_o + C_h \bar{A} \sum_c \phi_c \psi_c$$

where

$$\psi_c = \alpha + f_c \; (1+\beta_1\rho_c+\beta_2 R_c+\beta_3 Z_c).$$

$\alpha=C_l/C_h$ is the relative cost of land, $\beta_{1,2,3}$ are relative cost parameters for various kinds of wiring (i.e. relative to heliostat cost which is dominant), and ρ_c is the radius of the cell center relative to the tower.

The stationary condition states that

$$\delta C = F \; \delta E$$

for all possible variations, δ. Dimensionless expressions for total thermal energy and total thermal system cost are defined as

$$\Lambda = \sum_c \eta_c \lambda_c f_c \phi_c,$$

and

$$\Gamma = C/(C_h \bar{A}).$$

As previously, the cell matching parameter

$$\tilde{\mu} = C_h/(Fa\bar{S}).$$

After differentiation we can drop factors of ϕ_c, so that

$$\partial_{f_c} \Lambda = \eta_c(\lambda_c+f_c\partial_{f_c}\lambda_c)$$

$$\partial_{t_c} \Lambda = \eta_c(\partial_{t_c}\lambda_c)f_c$$

$$\partial_{\phi_c} \Lambda = \eta_c\lambda_c f_c$$

$$\partial_{f_c} \Gamma = 1+\beta_1\rho_c+\beta_2 R_c+\beta_3 Z_c+(\beta_2\partial_f R_c+\beta_3\partial_f Z_c)f_c$$

$$\partial_{t_c} \Gamma = (\beta_2\partial_t R_c+\beta_3\partial_t Z_c)f_c$$

$$\partial_{\phi_c} \Gamma = \alpha + f_c(1+\beta_1\rho_c+\beta_2 R_c+\beta_3 Z_c).$$

The stationary condition gives

$$C_h\bar{A}\ \delta\Gamma = Fa\bar{S}\bar{A}\ \delta\Lambda$$

or

$$\delta\Lambda = \tilde{\mu}\delta\Gamma.$$

Consequently,

$$\eta_c(\lambda_c+f_c\partial_f\lambda_c) = \tilde{\mu}\ \partial_{f_c}\Gamma$$

$$\partial_t\lambda_c = \tilde{\mu}\ (\beta_2\partial_t R_c+\beta_3\partial_t Z_c)/\eta_c$$

for interior cells, and

$$\eta_c\lambda_c = \tilde{\mu}\ (\alpha/f_c+1+\beta_1\rho_c+\beta_2 R_c+\beta_3 Z_c)$$

for boundary cells. B_c is defined as $\eta_c\lambda_c$ divided by the equivalent right side. As previously, the interior of the field satisfies the condition

$$B_c \equiv \eta_c\lambda_c/((\alpha/f_c+1+\beta_1\rho_c+\beta_2 R_c+\beta_3 Z_c)\tilde{\mu})\ \geq\ 1.$$

These relations degenerate to the previous case if land and wiring have no cost; i.e.,

$$\alpha = 0 = \beta_1 = \beta_2 = \beta_3.$$

2.3 Power Dependent Cost Model

In practice, it is also necessary to consider <u>power</u> dependent costs. For this purpose, the cost model becomes

$$C = C_o + C_p(P_o) + C_h\bar{A}\sum_c\phi_c\psi_c$$

where $C_p(P)$ is the power dependent term and P_o is the total thermal power at design time. In this case,

$$\delta F = (1/E)\delta C - (C/E^2)\delta E = 0$$

with

$$\delta C = \delta(C-C_p) + (\partial_p C_p)\delta P_o$$

and δE as previously given. $\partial_p C_p$ is known, but δP_o needs explanation.

Let $P(\tau)$ be the total thermal power at time τ. $P(\tau)$ can be expressed as

$$P(\tau) = a\sigma(\tau)\bar{A}\sum_c \eta_c \xi_c f_c \phi_c - b/\bar{H}$$

where $\xi_c = \xi_c(f_c, t_c)$ is the efficiency of heliostats in cell c for re-directed power at time τ and $\bar{H}$ is the number of useful hours in a year. The time dependent quantities are related to the corresponding annual quantities by integrating over the useful hours in an average year. In summary

$$\bar{H} = \int_H d\tau,$$

$$\bar{S} = \int_H d\tau\sigma(\tau),$$

$$\lambda_c = \int_H d\tau\sigma(\tau)\xi_c(\tau)/\bar{S},$$

and

$$E = \int_H d\tau P(\tau).$$

The variation of P_o is given by

$$\delta P_o = a\sigma(\tau_o)\bar{A}\eta_c\{\delta f_c(\xi_c + f_c\partial_f\xi_c)\phi_c + \delta t_c(\partial_t\xi_c)f_c\phi_c + \delta\phi_c\xi_c f_c\}.$$

δP_o can be used to derive optimum conditions. However, it is useful to assume that the incident energy is proportional to the incident power at design time. Let

$$E = a\, E_{inc} - b$$

$$P_o = p(\tau_o) = aP_{inc} - b/\bar{H}$$

and

$$E_{inc} = H_o\, P_{inc}$$

so that

$$\delta P_o = a\,\delta\, P_{inc} = (a/H_o)\, \delta E_{inc}$$

$$= (1/H_o)\, \delta E \quad .$$

The stationary condition

$$\delta C = F\delta E$$

gives

$$F\delta E = \delta(C-C_p) + (\partial_p C_p)\delta P_o \ .$$

Consequently,

$$F\delta E = \delta(C-C_p) + (\partial_p C_p)(1/H_o)\delta E$$

or

$$\delta(C-C_p) = F^*\delta E$$

with

$$F^* = F - (\partial_p C_p)/H_o .$$

The previous optimum conditions are applicable with $F \twoheadrightarrow F^*$ in $\tilde{\mu}$. Consequently, under the simplifying assumption for P_o, we can obtain power constrained optima by converging

$$F^*(\text{INPUT}) \twoheadrightarrow F^*(\text{OUTPUT}).$$

The previous input for F becomes F*(INPUT). New outputs are needed for H_o(OUTPUT) and F*(OUTPUT) with

$$H_o(\text{OUTPUT}) = E_{inc}/P_{inc}$$

and

$$F^*(\text{OUTPUT}) = C/E - (\partial_p C_p)P_{inc}/E_{inc} .$$

3. Transition to a Heliostat Layout using an Optimization with Fixed Azimuthal Spacings

The cellwise optimization method ignores geometrical constraints which occur at the cell boundaries. If these effects were rigorously included, an impossible N variable problem would occur. The nature of these difficulties can be seen when a cellwise optimum is converted to an actual heliostat layout (see figure 3.1). If we assume a circular layout, spacing between circles can be obtained from the cellwise optimum by making an azimuth independent fit on the optimum R_c values for the relevant cells. Optimum azimuthal spacings Z_c are nearly the same for all cells. Assume a reasonable azimuthal spacing Z_1 for all heliostats on the outer circle. For instance, let

$$Z_1 = \rho_1 \Delta\phi$$

where ρ_1 is the radius of the outer circle and $\Delta\phi$ is the azimuthal angle separating heliostats in the zone containing the outer circle. The n^{th} circle of this zone will have the azimuthal spacing

$$Z_n = \rho_n \Delta\phi = Z_1 (\rho_n/\rho_1)$$

so that the inner circles are squeezed into progressively smaller azimuths and for some n, an unacceptable amount of loss occurs. At this point a new zone must be created with

$$Z_{n+1} \cong Z_1.$$

We can assume that the average azimuth $\langle Z \rangle$ equals the optimum values for the zone, but a systematic departure from optimum occurs as we cross a zone. This systematic behavior of a zonal layout is ignored by the cellwise optimization in its original form (see Figures 3.2-3.4).

It is impractical to solve for the zone boundaries in the optimizer. However, a more balanced layout is possible by making better use of the

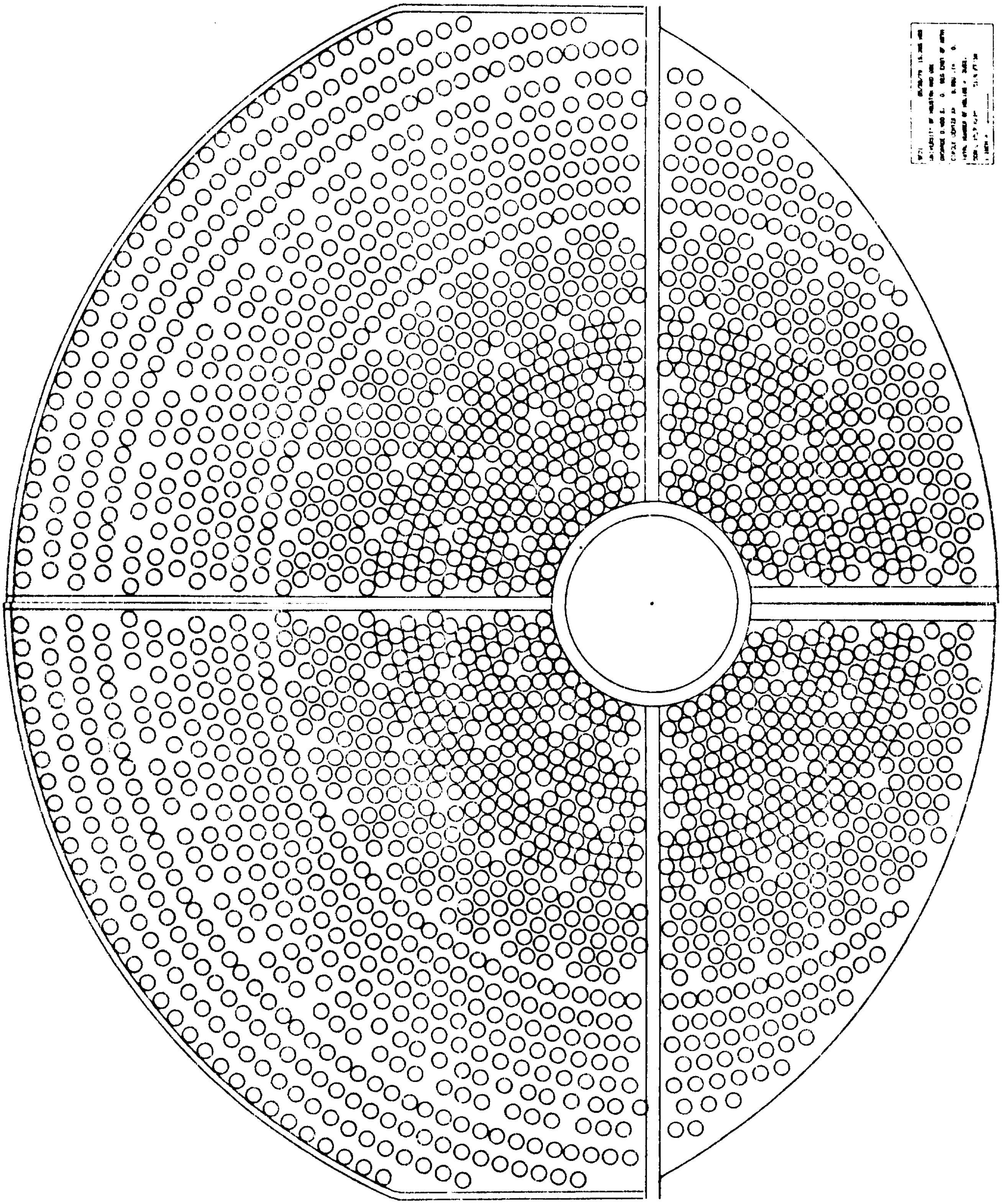

Figure 3.1 "Barstow" Heliostat Layout.

This version has 2062 heliostats confined to a prescribed region having a tower exclusion and four roads. There are six zones. Circles touching indicate mechanical limits. The deleted heliostats are conspicuous. The inner zone is nearly hexagonal closest packing.

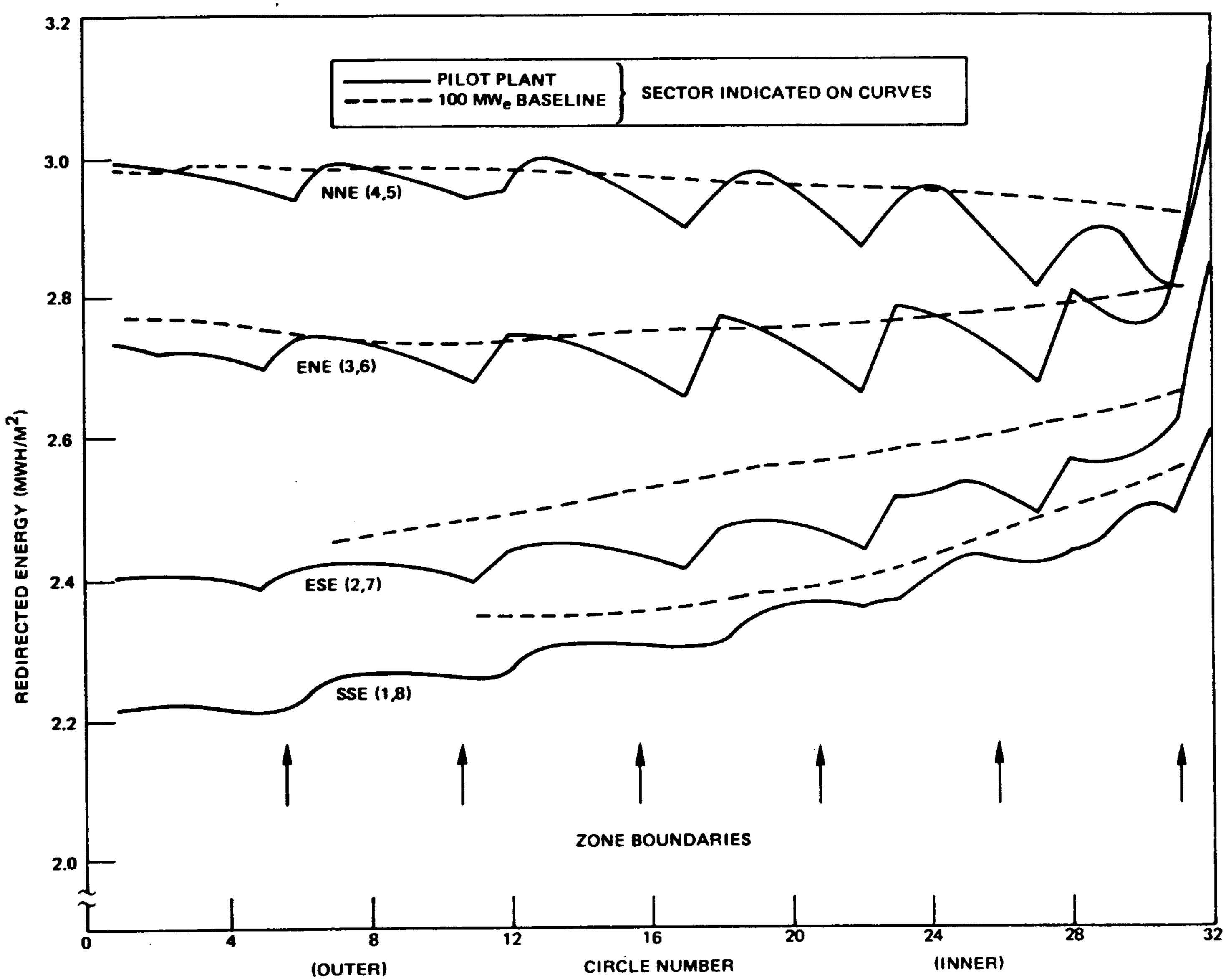
PILOT PLANT
100 MWe BASELINE
SECTOR INDICATED ON CURVES
NNE (4,5)
ENE (3,6)
ESE (2,7)
SSE (1,8)
ZONE BOUNDARIES
REDIRECTED ENERGY (MWH/M²)
3.2
3.0
2.8
2.6
2.4
2.2
2.0
0
4
8
12
16
20
24
28
32
(OUTER)
CIRCLE NUMBER
(INNER)

Figure 3.2 Redirected Energy Versus Circle Number.

The dotted line represents this 100 MW_e baseline power plant as output by the cellwise optimizer. The cellwise optimum field has no zone structure. The solid line represents the pilot plant as output by the individual heliostat performance model for an actual layout. The pilot plant was designed to resemble the 100 MW_e power plant. The layout has six zones. The four curves represent octants in the east half field. East-West symmetry exists. Circle 1 is the outer circle in figures 3.2 and 3.3.

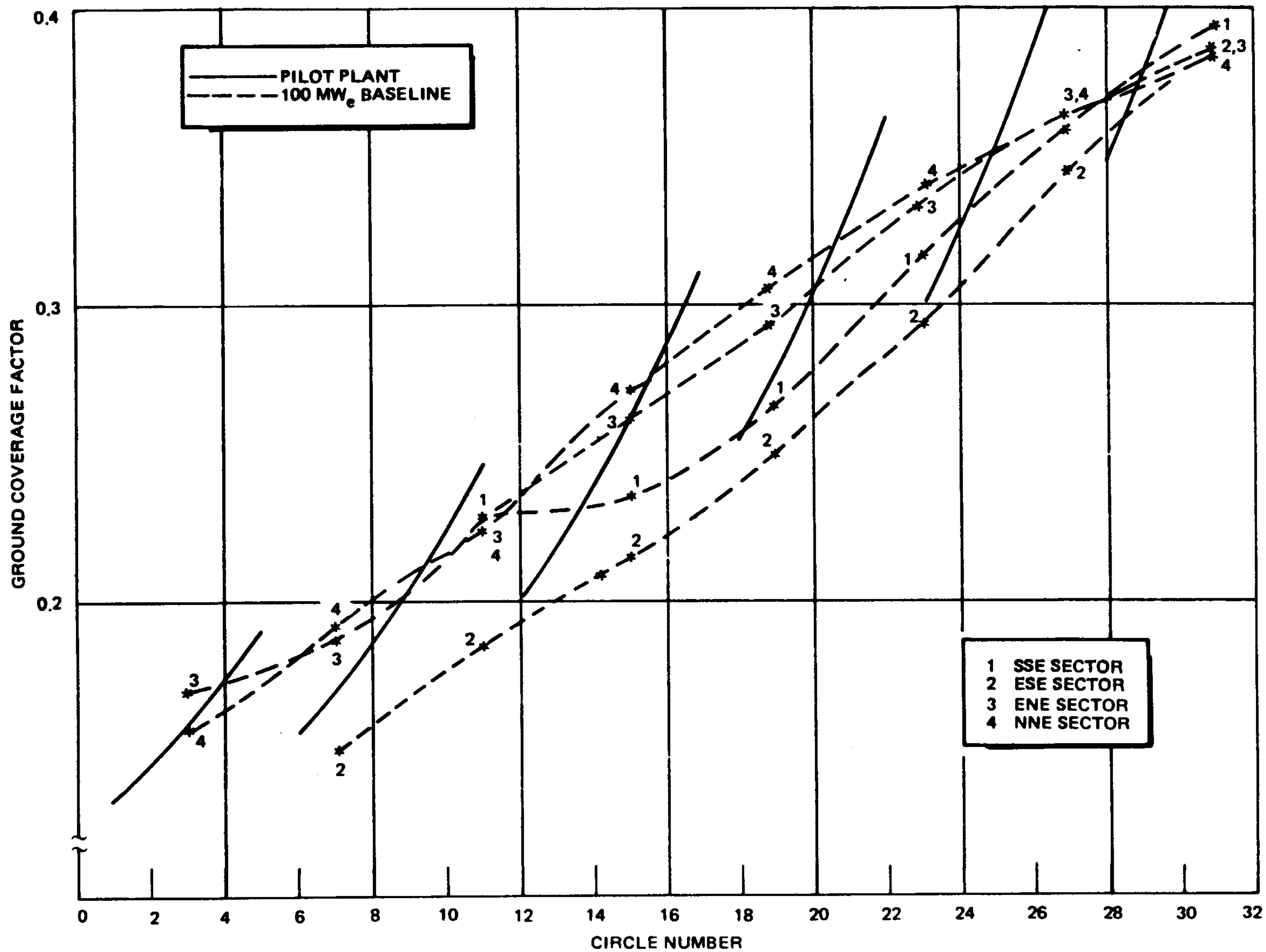

PILOT PLANT
100 MWe BASELINE
1 SSE SECTOR
2 ESE SECTOR
3 ENE SECTOR
4 NNE SECTOR
GROUND COVERAGE FACTOR
CIRCLE NUMBER
0.4
0.3
0.2
0
2
4
6
8
10
12
14
16
18
20
22
24
26
28
30
32

Figure 3.3 Ground Coverage Fraction versus Circle Number.

The solid lines represent a circular layout for a pilot plant having six zones. All octants have the same ground coverage because of the circular symmetry. Output from the cellwise optimizer for the corresponding 100 MW_e plant shows some deviations from circular symmetry and no zones.

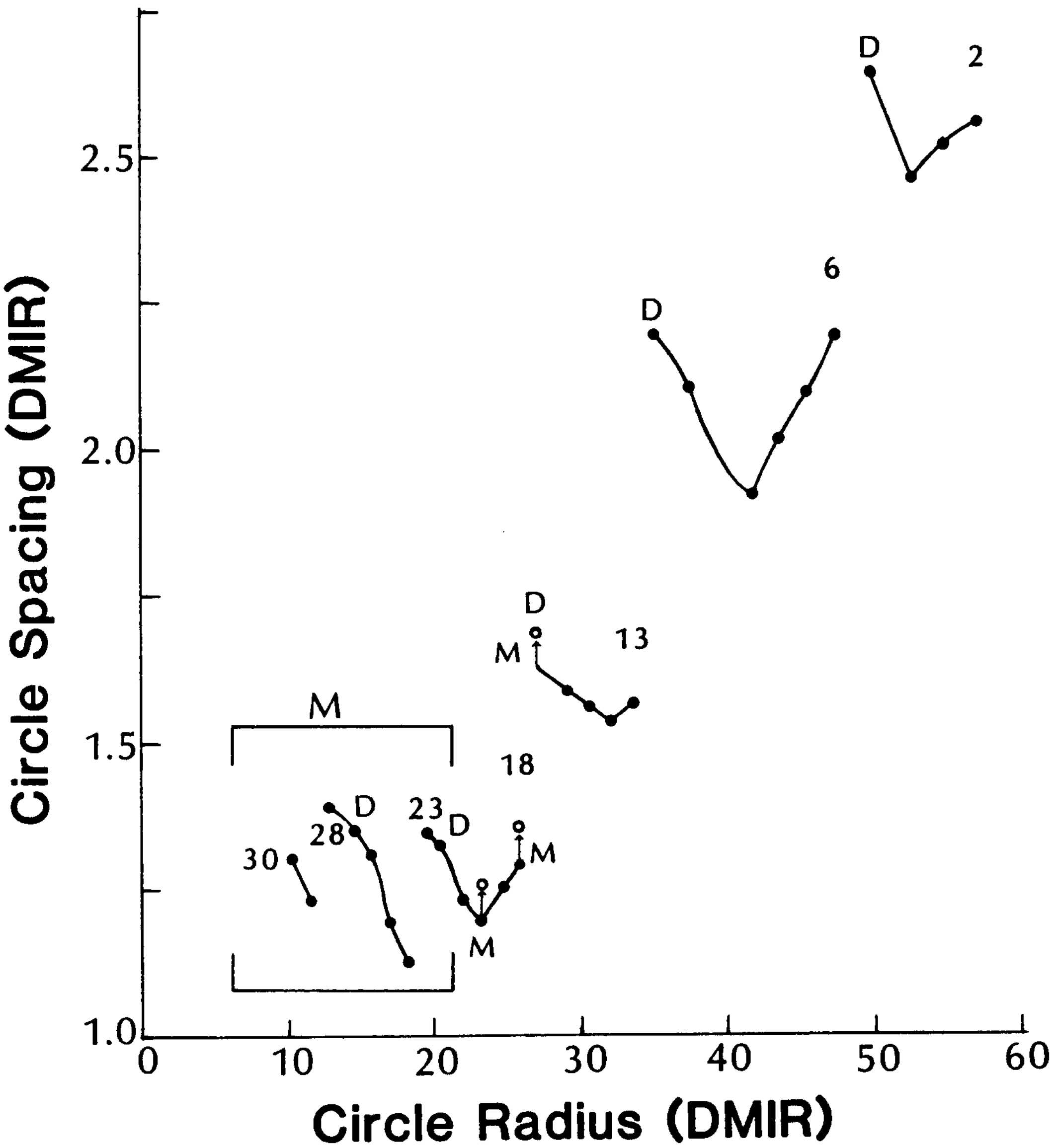

Figure 3.4 Circle Spacing versus Circle Radius.

This figure shows the performance of the circle generating subroutine. The connected line joins points belonging to a zone. R(I-1)-R(I) is plotted against R(I). The circle number of the first circle in each zone is shown over the point. D over a point indicates that deletes occur in this circle. An upward arrow with an M indicates that R(I) was decreased because of mechanical limits. The boxed region is entirely controlled by mechanical limits. The outer three zones show a V shape graph. The right branch of the V is primarily due to "nose blocking" (i.e., blocking due to the heliostat directly towards the tower and two circles inward). The left branch of the V is primarily due to diagonal blocking from the two heliostats one circle inward. Such diagonal blocking becomes more important as the azimuthal separation decreases, i.e., as one moves inward in a zone.

shading and blocking data. The optimization method described in section 2 requires the interpolated function

$$\lambda_c(R,Z) = \text{Fit}(R,Z;\ \lambda_c(R_i,Z_j) | i,j=1...4),$$

where

$$R_i = R'_c\ (1+(i-2\tfrac{1}{2})\delta_o),$$

and

$$Z_j = Z'_c\ (1+(j-2\tfrac{1}{2})\delta_o).$$

δ_o = 1/10 is a useful choice for the size of variations. (R'_c,Z'_c) are input estimates for the optimum (R_c,Z_c) (See Figure 3.5). The $\lambda_c(R_i,Z_j)$ are based on insolation and shading and blocking data. The improved layout function $\bar{R}(\rho,Z)$ gives

$$\rho_{n-2} = \rho_n - \bar{R}(\rho_n,Z_n)$$

where ρ_n is the radius of the n^{th} circle measured in the plane of the heliostat field and Z_n is the azimuthal spacing in the n^{th} circle of the zone.

The improved layout function is defined as follows. Let

$$\bar{R}(\rho,Z) = \text{Cubic Fit } (Z;\ \tilde{R}(\rho,Z_i) | i=1..4)$$

where

$$\tilde{R}(\rho,Z_i) = \text{Quadratic WLS } (\rho;\ \hat{R}_c(\rho_c,Z_i) | c\varepsilon\text{field})$$

and $\hat{R}_c(\rho_c,Z_i)$ = Optimum value of R_c with Z_c constrained to Z_i. The $\hat{R}_c(p_c,Z_i)$ are obtained from CELLAY.

The CELLAY solution for $\hat{R}_c$ is similar to the method used for (R_c,Z_c) except that one less variable occurs. In this case, we have

$$\partial_{R_c} C = F\partial_{R_c} E$$

and

$$\partial_{\phi_c} C = F\partial_{\phi_c} E.$$

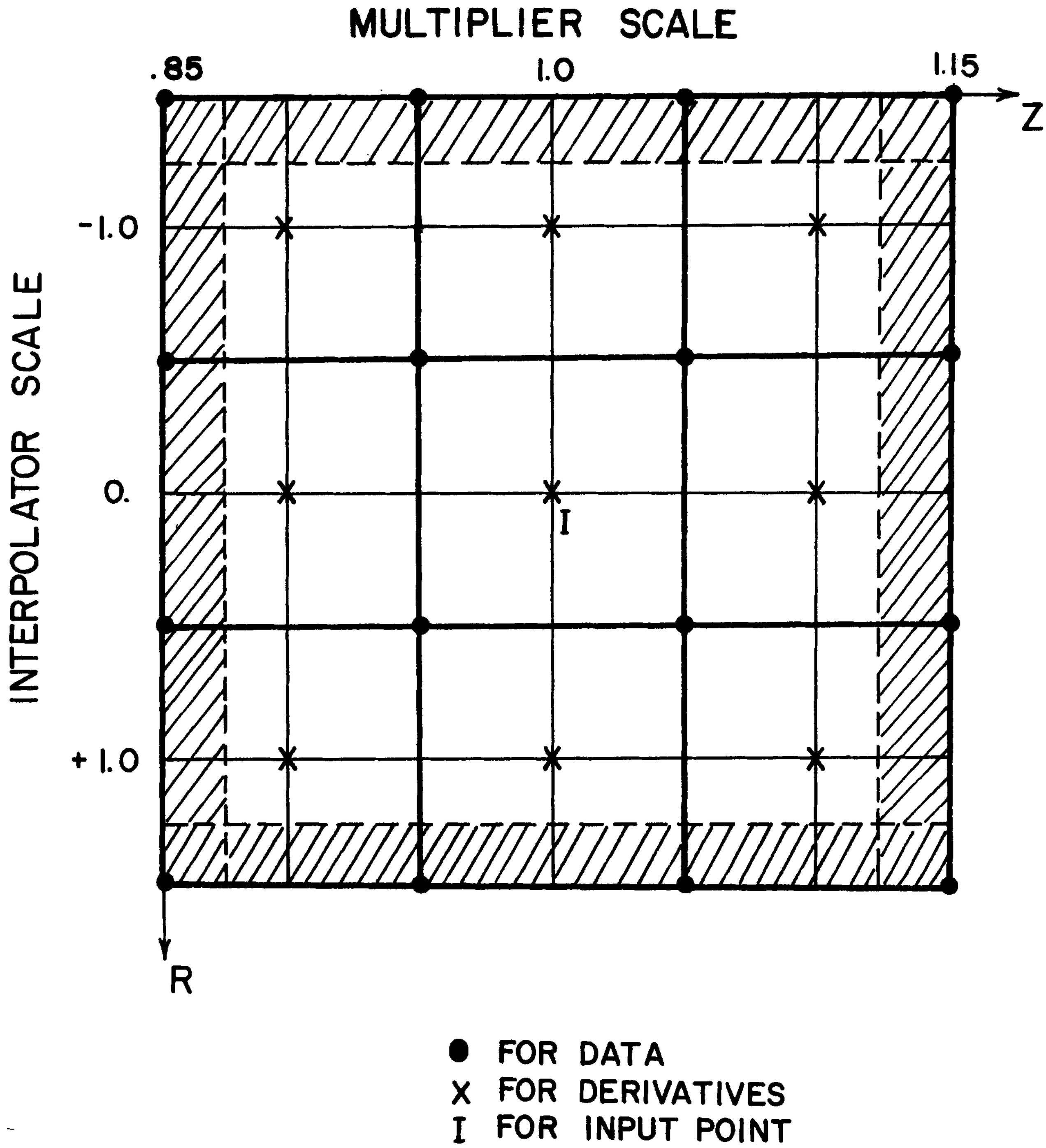

3.5 Interpolation in the (R,Z) Patch.

This is the region spanned by variations of (R_c,Z_c). Sixteen data points and nine intermediate points are used to support a quadratic fit on the two dimensional region. The solution finder refuses to go into the shaded region except for special default cases. This whole region is represented as a rectangle in Figure 2.6.

Using the land and wiring cost model, we have

$$\partial_{R_c} C = C_h\bar{A} \{ -(f_c/R_c)(1+\beta_1\rho_c+\beta_2R_c+\beta_3Z_c) + \beta_2f_c\}$$

$$\partial_{\phi_c} C = C_h\bar{A}\psi_c$$

$$\partial_{R_c} E = a\bar{S}\bar{A}\eta_c(R_c\partial_{R_c}\lambda_c-\lambda_c)(f_c/R_c)$$

$$\partial_{\phi_c} E = a\bar{S}\bar{A}\eta_c\lambda_cf_c$$

Consequently,

$$\eta_c(R_c\partial_{R_c}\lambda_c-\lambda_c) = (C_h/Fa\bar{S})\ \{\beta_2R_c-(1+\beta_1\rho_c+\beta_2R_c+\beta_3Z_c)\}$$

for all interior cells, and as previously

$$B_c = \eta_cf_c\lambda_c/(\psi_c\tilde{\mu}) = 1$$

for boundary cells.

4. Optimization with Boundary Constraints

Boundary constraints can be introduced via the assumption that

$$\phi_c = 0 \text{ for } c \in \bar{B} \qquad \text{(i.e. C belongs to set } \bar{B}\text{)}$$

where $\bar{B}$ is the fixed set of exterior cells. Consequently,

$$E = a\bar{A}\bar{S} \left(\sum_{c \in B} \eta_c \lambda_c f_c \phi_c \right) - b$$

where B is the set of allowed cells. The optimized field may fill any subset of B.

If boundary constraints are extreme, the power available for a "reasonable" tower height may be very low, leading to an unreasonably high figure of merit. In such cases use of a taller tower (50 to 100% taller) will reduce blocking losses and may allow enough extra heliostats in the constrained area to result in a lower figure of merit. This approach also delivers more power from the same land area. Thus, boundary constraints can lead to various results. (See Figures 4.1 and 4.2.)

```
NGON =   4  ; MAX. NUMBER OF HELIOS./CELL=    12.8   ; HGLASS/DMIR**2 =  0.9567   ; TOTAL GLASS = 0.14016E 05
                                  247. HELIOS    AHELI=  56.8419    ASEG=  56.8419   ; TOTAL LAND  = 0.48296E 05

F-LIMIT      OPTIMUM       ALLOWED      M-LIMIT

  00000000000   00000000000   00000000000   000000
  00000000000   00000100000   00000000000   000000
  00000000000   01233433210   00000000000   000000
  00000000000   21444444412   00000000000   000000
  00022100000   44444444444   00022100000   000000
  00014443321   44444444444   00014443321   000000
  00144444443   44444444444   00144444443   000000
  00244444441   44444444444   00244444441   000000
  00244444440   44444444444   00244444440   000000
  00344444430   44444444444   00344444430   000000
  00344444410   44444444444   00344444410   000000
  00444444400   44444444444   00444444400   000000
  00444444300   44444444444   00444444300   003000
  00144444000   34444444443   00144444000   330300
  00003230000   00444444400   00003230000   332000
  00000000000   00000000000   00000000000   000000

* * * * * * * * * * * * * * NUMBER OF HELIOSTATS PER CELL* * * * * * * * * * * * * ; HT =   54.0 METERS FOCAL HEIGHT
                                                                                   RECEIVER LENGTH =   7.0 M; WIDTH =   7.0 M.
              THE RECEIVER IS APERTURED BY AN ELLIPTICAL APERTURE   5.00 M WIDE AND   5.00 M HIGH

   0.     0.     0.     0.     0.     0.     0.     0.     0.     0.     0.
   0.     0.     0.     0.     0.     0.     0.     0.     0.     0.     0.
   0.     0.     0.     0.     0.     0.     0.     0.     0.     0.     0.
   0.     0.     0.     0.     0.     0.     0.     0.     0.     0.     0.
   0.     0.     0.     1.0    1.0    0.5    0.     0.     0.     0.     0.
   0.     0.     0.     2.3    2.3    2.3    2.3    1.7    1.7    1.1    0.5
   0.     0.     0.6    2.5    2.6    2.6    2.6    2.5    2.4    2.3    1.7
   0.     0.     1.4    2.8    2.9    2.9    2.9    2.8    2.7    2.6    0.6
   0.     0.     1.5    3.2    3.2    3.3    3.2    3.2    3.0    2.9    0.
   0.     0.     2.5    3.6    3.7    3.7    3.7    3.6    3.4    2.4    0.
   0.     0.     2.9    4.1    4.2    4.3    4.2    4.1    3.8    0.9    0.
   0.     0.     4.3    4.7    5.0    5.1    5.0    4.7    4.3    0.     0.
   0.     0.     4.9    5.3    5.1    5.2    5.1    5.3    3.6    0.     0.
   0.     0.     1.3    5.3    6.0    6.0    6.0    5.3    0.     0.     0.
   0.     0.     0.     0.     4.5    3.0    4.5    0.     0.     0.     0.
   0.     0.     0.     0.     0.     0.     0.     0.     0.     0.     0.

PERFORMANCE SUMMARY AND COST BREAKDOWN FOR OPTIMIZED COLLECTOR FIELD - TRIM LINE AT  1.000

    EQNOON POWER      =    8.809     9.075IN MW - (SCALED TO  940.0W/M2)
    ANNUAL ENERGY     =   13.924 IN GWH
    FIXED COSTS       =    0.5000 IN $M
    TOTAL TOWER COST=      2.1968; TOW  0.4532; REC  1.7109; V P  0.0099; PUMP  0.0229 IN $M FOR  940.0 EQUINOON POWER
    SUM PV O&M COSTS=      1.3436;      0.1029;      0.3884;      0.    ;        0.8524; PV OF O&M COSTS IN $M
    LAND COST         =    0.      IN $M;  PV OF O&M COST = 0.      IN $M
    WIRING COST       =    0.0659 IN $M;  PV OF O&M COST = 0.      IN $M
    HELIOSTAT COST    =    3.7283 IN $M;  PV OF O&M COST = 3.7344 IN $M
    CAPITAL COST TOT=      6.4909 IN $M;  PV O&M COST TOT= 5.0780 IN $M
    GRAND COST TOTAL=     11.5690 IN $M
    FIGURE OF MERIT =    830.882 IN $/MWH , FOR AN INPUT FM OF 650.000
```

Figure 4.1 Output for an Asymmetric Boundary.

The ALLOWED block of integers is input to define the constraint on land use. The choice (0,1,2,3,4) corresponds to (0,1/4,1/2,3/4,1) times the available area for each cell. After optimization, the number of heliostats/cell is given by the array in the middle of the page directly above the summary output.

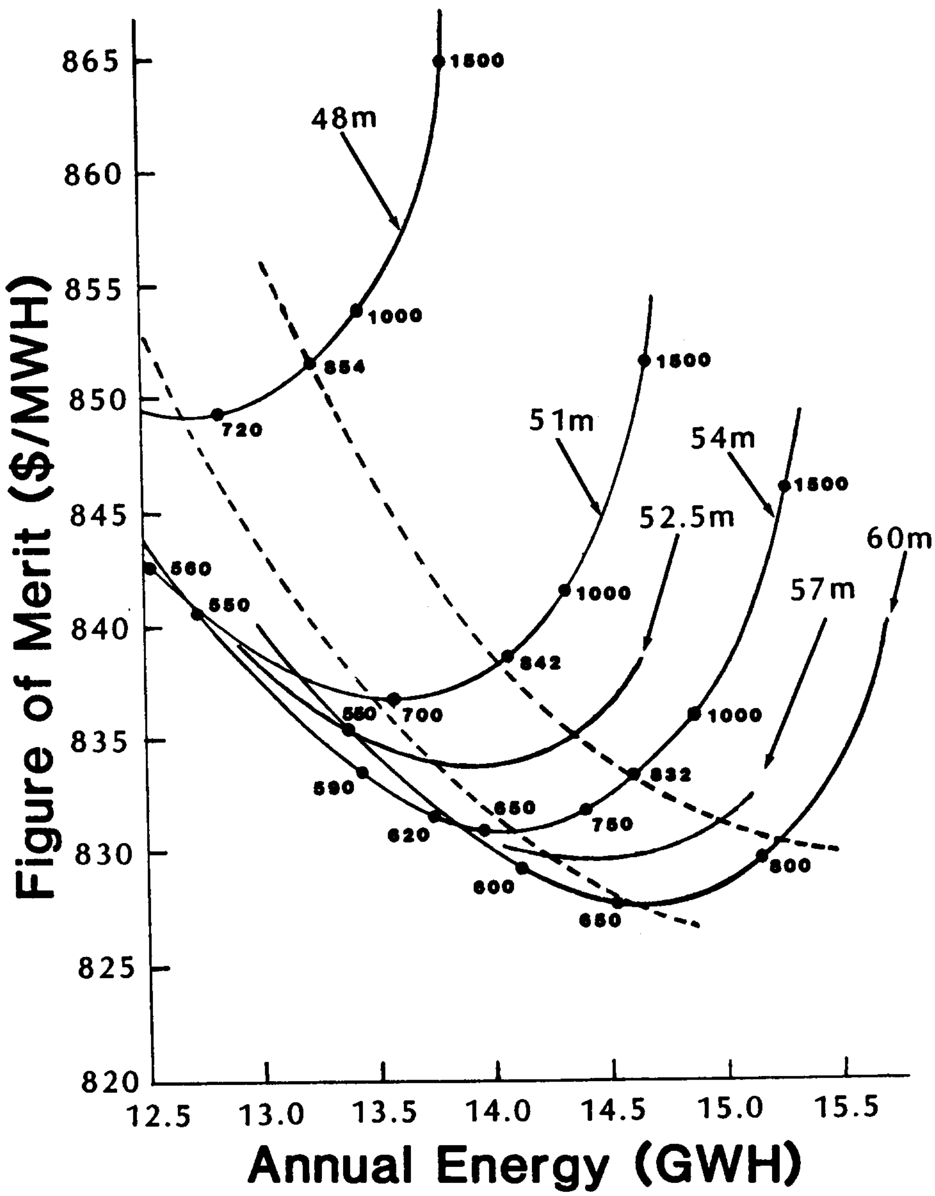

Figure 4.2 Figure of Merit versus Annual Energy.

Each curve corresponds to a tower height. Numbers next to the circled points are input figures of merit. The two dashed curves correspond to the locus of minima and the locus of converged optima. Convergence (i.e., input figure of merit = output figure of merit) will occur at the minimum of each curve except for the effect of power dependent cost. The steeply rising portion of the curves on the right represents nonproductive overcrowding of the availible space.

5. Optimization with Mechanical Constraints for Heliostat Rotation

If all heliostats are tracking accurately, the planes of neighboring heliostats are nearly parallel and no collisions are likely. However, during startup or shutdown operations, or if a few heliostats are disabled, the parallelism of neighbors will not be maintained and it is necessary that the heliostat layout satisfies a free turning mechanical constraint. Figure 5.1 shows a portion of the radial stagger neighborhood. Free turning imposes three different mechanical limits known as the radial, azimuthal, and diagonal limits. The free turning condition is represented by the diameter of the sphere generated by the rotation of the heliostat plus a safety margin. Let D_M represent the diameter of the safe sphere. In practice a typical value is

$$D_M = 1.5362\ D_H.$$

Figure 2.6 shows the appearance of the three mechanical limits in the (R,Z) plane. Figure 5.1 also shows the allowed region which is defined by the inequalities

$$R \geq D_M,$$

$$Z \geq D_M,$$

and

$$(R/2)^2+(Z/2)^2 \geq D_M^2.$$

When an optimum collector geometry is determined as in section 2, some of the cells may have solutions falling in the unallowed region. The three constraints are separated by the two points of hexagonal closest packing marked H_1 and H_2 in Figure 5.1. C_o is the mid point of B_2 in figure 5.1. C_o is also the point of minimum ground coverage on B_2 (see Figure 5.2).

It is easy to see that at

$$H_1:\quad Z_1 = D_M;\quad R_1 = \sqrt{3}D_M;\quad \chi_1 = \tan^{-1}(1/\sqrt{3});$$
$$f_1 = a_c/\sqrt{3}D_M^2;\quad t_1 = \tfrac{1}{2}(3D_M^2 - D_M^2) = D_M^2$$

$$H_2:\quad Z_2 = \sqrt{3}D_M;\quad R_2 = D_M;\quad \chi_2 = \tan^{-1}(\sqrt{3});$$
$$f_2 = a_c/\sqrt{3}D_M^2;\quad t_2 = \tfrac{1}{2}(D_M^2 - 3D_M^2) = -D_M^2$$

and

$$C_o:\quad Z = \sqrt{2}D_M;\quad R = \sqrt{2}D_M;\quad \chi = \pi/4;$$
$$f = a_c/RZ = a_c/2D_M^2;\quad t = 0.$$

If the unconstrained optimum falls outside the allowed region, the solution must be moved to a point on the boundary of the allowed region. The boundary of the allowed region has the following branches:

$$(\infty,H_1)_{B_3},\quad (H_1,H_2)_{B_2},\quad \text{and}\quad (H_2,\infty)_{B_1}.$$

The optimum choice of boundary points is the point of minimum F. If the minimum occurs on $(\infty,H_1)_{B_3}$, then

$$\partial_R F = 0$$

is necessary unless the minimum occurs at the end point H_1. If the minimum occurs on $(H_1,H_2)_{B_2}$, then

$$\partial_\chi F = 0$$

is necessary unless H_1 or H_2 is the solution. Similarly, if the minimum occurs on $(H_2,\infty)_{B_1}$, then

$$\partial_Z F = 0$$

is necessary unless the minimum is H_2.

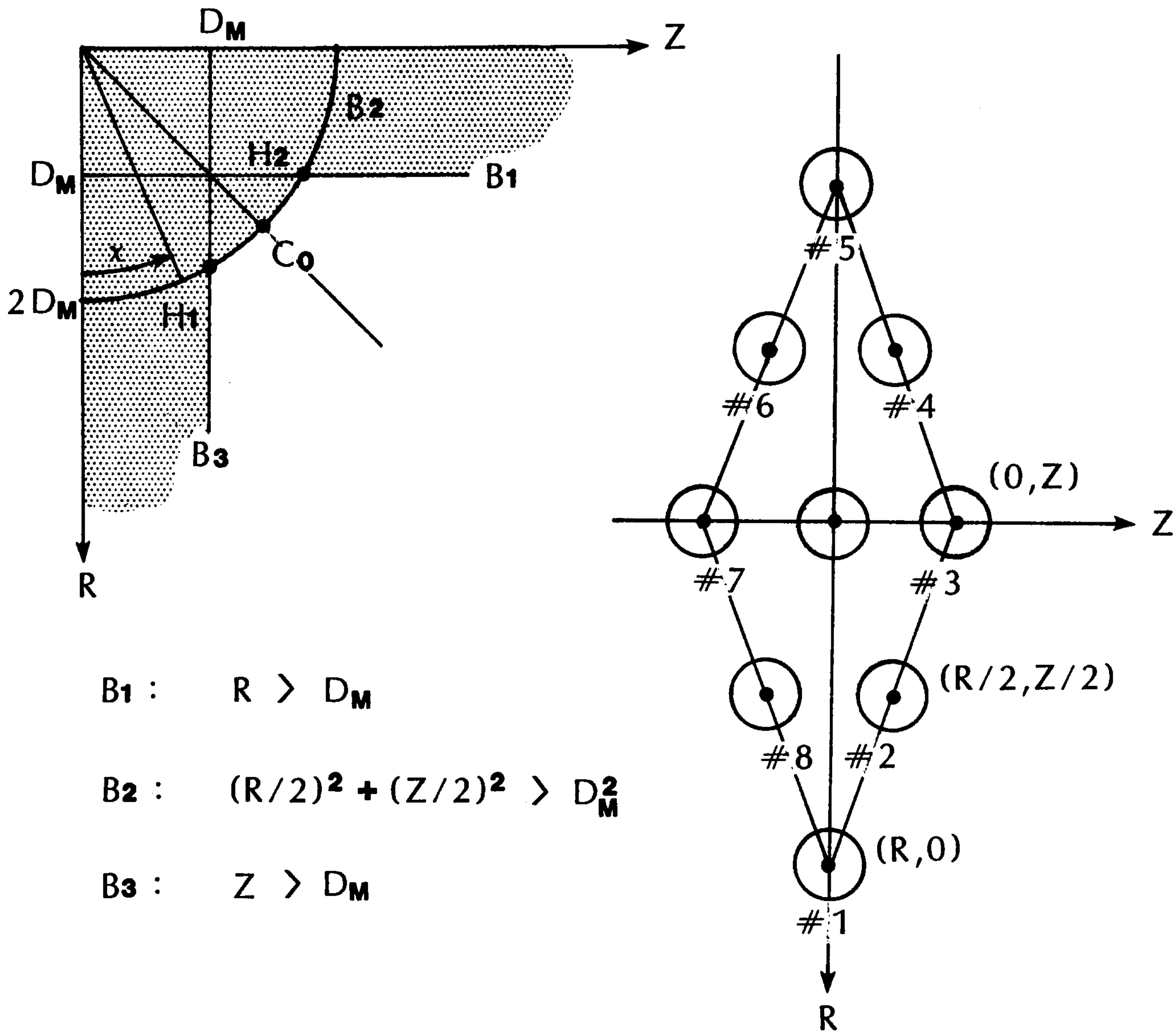

Figure 5.1 Radial Stagger Neighborhood and Mechanical Limits.

R is the radial coordinate and Z is the azimuthal coordinate. Circles represent the excluded sphere for each heliostat. The circle at the origin is the central heliostat. Heliostats 1 to 8 are the closest neighbors. Heliostat #1 is nearest to the tower and will cause serious blocking losses if R is small. Heliostats 4 to 6 are symmetrically located but can not cause blocking. The free turning requirement relates the central heliostat to all of its nearest neighbors. Note that if Z is large and R is small, heliostat 1 becomes a nearest neighbor.

There are three mechanical limits: B_1 is the radial limit; B_2 is diagonal; and B_3 is azimuthal. The shaded region is not allowed. H_1 and H_2 are points of hexagonal closest packing and C_0 is the point of maximum ground coverage on B_2. The angle χ is a parameter for locating this constrained optimum in $[H_1, H_2]$ of B_2. See figure 5.2.

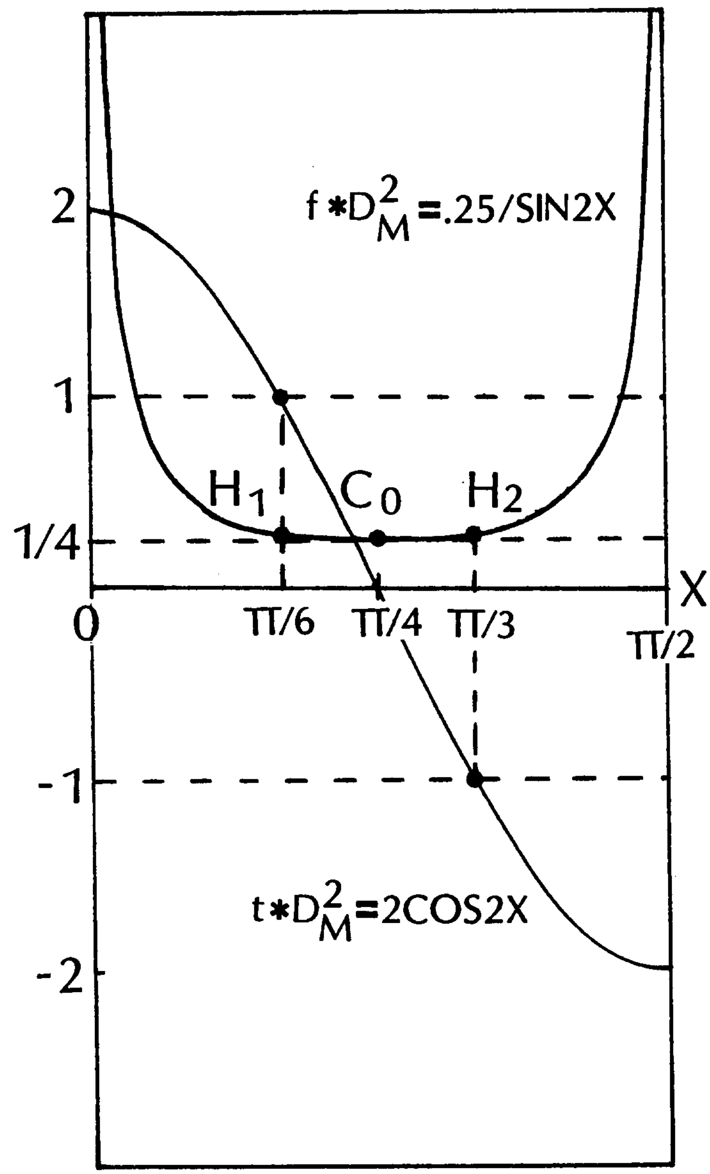

Figure 5.2 Graph of (f,t) versus χ on B_3.

The upper curve shows that C_o is the point of minimum f on B_3. We assume $a_c = 1/2$. The lower curve shows that t is a monotone parameter on B_3.

In practice, we assume that $\partial_R F>0$ on B_3 so that H_1 is the only possible minimum of B_3 and, similarly, $\partial_Z F>0$ on B_1 so that H_2 is the only possible minimum of B_1. This leaves the circular branch $(H_1,H_2)_{B_2}$ including the endpoints. Let

$$\partial_\chi F = \partial_\chi f \; \partial_f F + \partial_\chi t \; \partial_t F \qquad \text{(Eq. 5.1)}$$

where

$$\begin{aligned} \partial_\chi f &= \partial_\chi (a_c/(4D_M^2 \cos\chi \sin\chi)) \\ &= a_c/R^2 - a_c/Z^2 = a_c(Z^2-R^2)/R^2Z^2 \\ &= -2tf^2/a_c \end{aligned}$$

and

$$\begin{aligned} \partial_\chi t &= (4D_M^2/2)\; \partial_\chi(\cos^2\chi - \sin^2\chi) \\ &= -2RZ = -2a_c/f. \end{aligned}$$

For $\partial = \partial_{f_c}$ or ∂_{t_c}, we have

$$\partial F = (1/E)\; \partial C - (C/E^2)\; \delta E$$

and with $\phi_c=1$

$$\partial E = a\bar{S}\bar{A}\eta_c(\lambda_c \partial f_c + f_c \partial \lambda_c).$$

Consequently,

$$-E/(Fa\bar{S}\bar{A}\eta_c)\; \partial F = \lambda_c \partial f_c + f_c \partial\lambda_c + T_\partial \qquad \text{(Eq. 5.2)}$$

with

$$T_\partial = -\partial C/(Fa\bar{S}\bar{A}\eta_c).$$

We assume the land and wiring cost formula

$$C = C_o + C_h \bar{A} \sum_c \phi_c \psi_c$$

with

$$\psi_c = \alpha + f_c(1+\beta_1\rho_c+\beta_2 R_c+\beta_3 Z_c)$$

so that

$$\partial C = C_h \bar{A}\; \partial\psi_c$$

with $\phi_c=1$ for interior cells. This gives

$$T_\partial = (\tilde{\mu}/\eta_c)\ \partial\psi_c$$

where, as previously,

$$\tilde{\mu} = C_h/(Fa\bar{S}).$$

The evaluation of $\partial\psi$ requires $\partial(R,Z)/\partial(f,t)$ which is obtained by inverting $\partial(f,t)/\partial(R,Z)$. We know that

$$\begin{pmatrix} \partial_R f & \partial_R t \\ \partial_Z f & \partial_Z t \end{pmatrix} = \begin{pmatrix} -f/R & R \\ -f/Z & -Z \end{pmatrix}$$

so that

$$\begin{pmatrix} \partial_f R & \partial_f Z \\ \partial_t R & \partial_t Z \end{pmatrix} = \begin{pmatrix} -Z & -R \\ +f/Z & -f/R \end{pmatrix} \frac{RZ}{(R^2+Z^2)f}$$

$$= (R^2+Z^2)^{-1} \begin{pmatrix} -a_c Z/f^2 & -a_c R/f^2 \\ R & -Z \end{pmatrix}.$$

Consequently,

$$\partial_f\psi = 1+\beta_1\rho_c+\beta_2 R_c+\beta_3 Z_c$$
$$-(a_c/f(R^2+Z^2))\ (\beta_2 Z+\beta_3 R)$$

and

$$\partial_t\psi = +(f/(R^2+Z^2))\ (\beta_2 R-\beta_3 Z).$$

Equation 5.2 is now complete. Hence, $\partial_\chi F$ can be evaluated using Equation 5.1. Choosing

$$\partial_\chi F = 0$$

implies that

$$\partial_t F = tf(f/a_c)^2\ \partial_f F,$$

which can and will occur for both minima and maxima.

$$\partial_\chi F(H_1) > 0$$

implies a local minima at H_1, and

$$\partial_\chi F(H_2) < 0$$

implies a local minima at H_2.

In the computer implementation, we evaluate

$$\Sigma(\chi) = \text{Sign} \{[E/(Fa\bar{S}\bar{A}\eta_c)]\partial_\chi F\} = \chi/|\chi|$$

on a circle through the solution. If the unconstrained optimum falls outside of the allowed region, then the solution moves out to B_2. If the unconstrained optimum is allowed, then

$$(R^2+Z^2)^{\frac{1}{2}} > 2D_M.$$

Several cases occur. (See Figure 5.3).

Case 1)

$\Sigma(\chi)$ = + everywhere on B_2, then H_1 is the optimum solution.

Case 2)

$\Sigma(\chi)$ = - everywhere on B_2, then H_2 is the optimum solution.

Case 3)

$$\Sigma(\chi) = \begin{cases} + \text{ for } \chi < \chi_o \\ - \text{ for } \chi > \chi_o, \end{cases}$$

where χ_o is a maximum of F. Hence, $\chi = \chi_o$ can not be an optimum solution. In this case we arbitrarily assume that

H_1 is optimum if $\chi_o > 45°$,

H_2 is optimum if $\chi_o < 45°$.

Case 4)

$$\Sigma(\chi) = \begin{cases} - \text{ for } \chi < \chi_o \\ + \text{ for } \chi > \chi_o, \end{cases}$$

where χ_o is a minimum of F and $\chi = \chi_o$ can be accepted as an optimum solution.

Case 5)

If $\Sigma(\chi)$ changes sign several times, the automatic method fails. In most cases, when mechanical limits occur, $\Sigma(\chi)$ locates the optimum solution on B_2, and if no mechanical limits occur, it verifies the standard unconstrained solution. Figures 5.4-5.6 show output for a number of the cases discussed here.

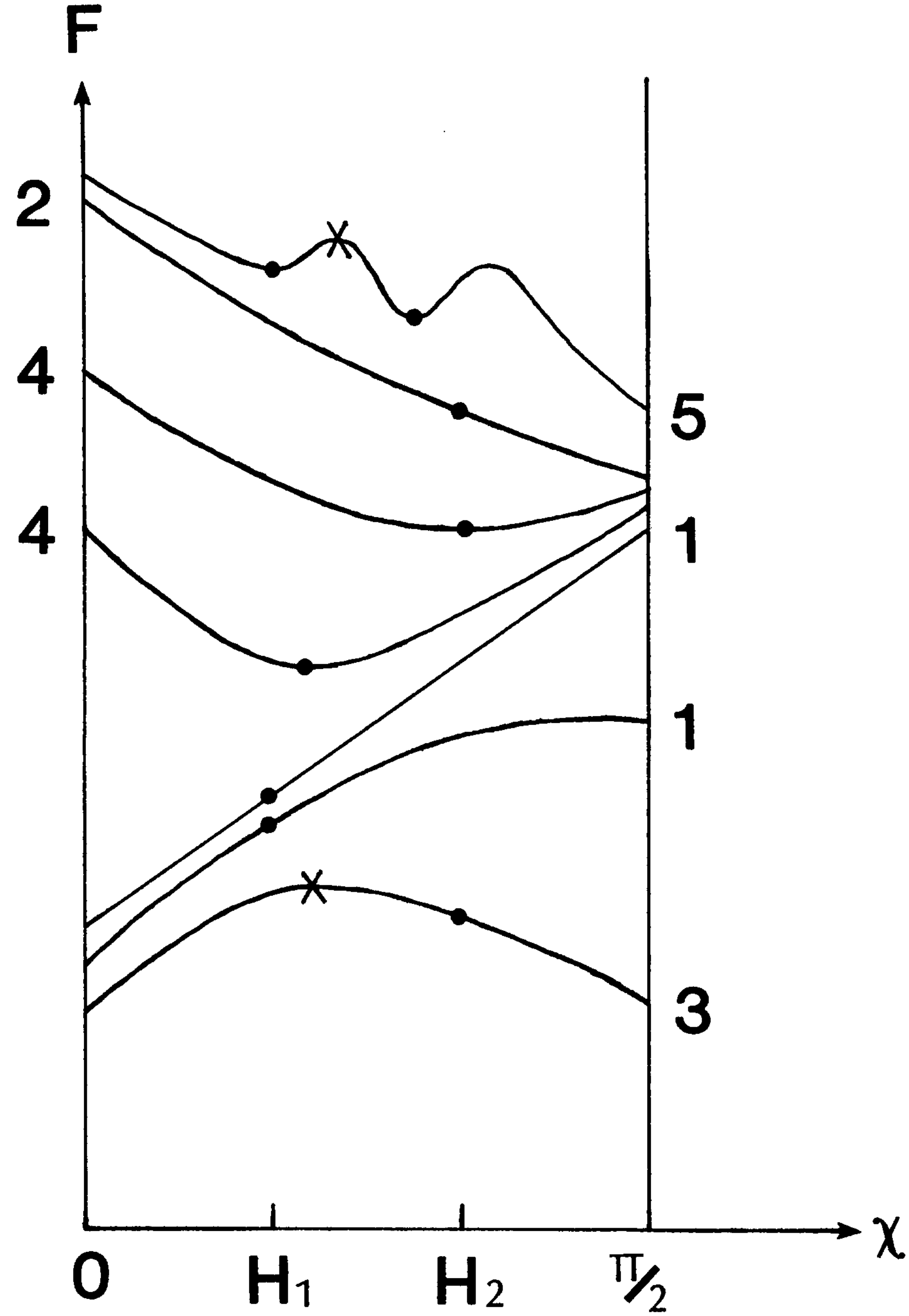

Figure 5.3 Figure of Merit versus χ for Five Cases.

The five cases are discussed in the text. X marks a maxima and dot marks a minima. The code deals with cases 1 to 4 automatically, but case 5 may require an operator judgement. An over-ride input is available for these rare cases.

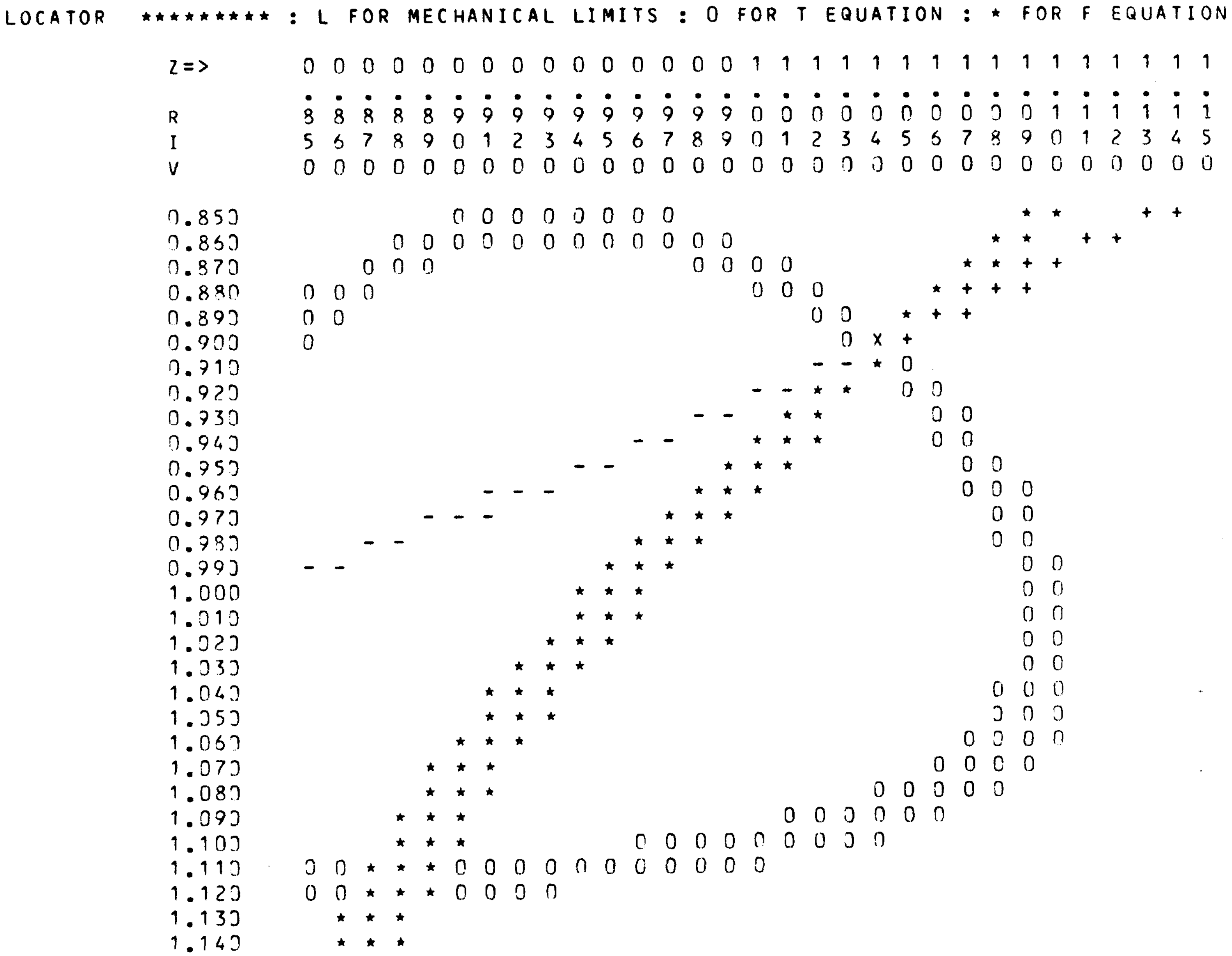

Figure 5.4 Finding the Correct Solution.

(R,Z) coordinates are given in multiplicative form. (1,1) is the input estimate. X marks the solution. 0 marks points where the t-equation holds and * marks the points where the f equation holds. In this case no mechanical limits occur in the zone of variations, but an alternative solution occurs in lower left. The circle of signs is always passed through the solution point. + on right of X and - on left of X verifies that the solution is minimum of the figure of merit. The +'s and -'s refer to the sign of $\Sigma(\chi)$. The ± are placed on a circle in the (R,Z) plane which is called the circle of signs.

```
LOCATOR  ********* : L FOR MECHANICAL LIMITS : 0 FOR T EQUATION : * FOR F EQUATION :

      Z=>    0 0 0 0 0 0 0 0 0 0 0 0 0 0 0 1 1 1 1 1 1 1 1 1 1 1 1 1 1 1 1
             . . . . . . . . . . . . . . . . . . . . . . . . . . . . . . .
      R      8 8 8 8 8 9 9 9 9 9 9 9 9 9 9 0 0 0 0 0 0 0 0 0 0 1 1 1 1 1 1
      I      5 6 7 8 9 0 1 2 3 4 5 6 7 8 9 0 1 2 3 4 5 6 7 8 9 0 1 2 3 4 5
      V      0 0 0 0 0 0 0 0 0 0 0 0 0 0 0 0 0 0 0 0 0 0 0 0 0 0 0 0 0 0 0

      0.850  L L L L L L L L L L L L L L L L L L L L L L L L L L L L L L L
      0.860  L L L L L L L L L L L L L L L L L L L L L L L L L L L L L L L
      0.870  L L L 0 L L L L L L L L L L L L L L L L L L L L L L L L L L L
      0.880  L L L L 0 L L L L L L L L L L L L L L L L L L L L L L L L L L
      0.890  L L L L L L L L L L L L L L L L L L L L +
      0.900  L L L L L L L L L L L L L L L L L L L +
      0.910  L L L L L L L L L L L L L L L L L L L + * * * *
      0.920  L L L L L L L L L L L L L L L L * * + +
      0.930  L L L L L L L L 0 L L L L L * * L L +
      0.940  L L L L L L L L L 0 L L * * L L L L +
      0.950  L L L L L L L L L L(*)* L L L L L +
      0.960  L L L L L L L L L * * 0 L L L L L +
      0.970  L L L L L L L L * L L L 0 L L L(X)
      0.980  L L L L L L L * L L L L L 0 L L -
      0.990  L L L L L L * * L L L L L L L -
      1.000  L L L L L L * L L L L L L L L -
      1.010  L L L L L * L L L L L L L L - -
      1.020  L L L L * * L L L L L L L L -   0
      1.030  L L L L * L L L L L L L L - -
      1.040  L L L * * L L L L L L L L -       0
      1.050  L L L * L L L L L L L L - -       0
      1.060  L L L * L L L L L L L L -         0
      1.070  L L * L L L L L L L L - -         0
      1.080  L L * L L L L L L L L -           0
      1.090  L L * L L L L L L L - -         0
      1.100  L L * L L L L L L L -         0
      1.110  L * L L L L L L L - -       0
      1.120  L * L L L L L L L -       0
      1.130  L * L L L L L L -       0
      1.140  L * L L L L L L -   0
      1.150  L * L L L L L - 0
```

Figure 5.5 Finding the Solution of B_3.

The L filled region is not allowed due to mechanical limits. This case shows B_1 and B_3. An ordinary solution occurs at the intersection of the zeros and stars, which happens to fall inside of mechanically limits. Therefore the solution is shifted to the position labeled X which is on B_3 at the point where the sign of $\Sigma(\chi)$ changes.

LOCATOR ********* : L FOR MECHANICAL LIMITS : 0 FOR T EQUATION : * FOR F EQUATION :

Z=> RIV	0.850	0.860	0.870	0.880	0.890	0.900	0.910	0.920	0.930	0.940	0.950	0.960	0.970	0.980	0.990	1.000	1.010	1.020	1.030	1.040	1.050	1.060	1.070	1.080	1.090	1.100	1.110	1.120	1.130	1.140	1.150
0.850	L	L	L	L	L	L	L	*	L	L	L	L	L	L	L	L	L	L	L	L	L	L	L	L	L	L	L	L	L	L	L
0.860	L	L	L	L	L	L	*	L	L	L	0	L	L	L	L	L	L	L	L	L	L	L	L	L	L	L	L	L	L	L	L
0.870	L	L	L	L	L	*	L	L	L	L	0	L	L	L	L	L	L	L	L	L	L	L	L	L	L	L	L	L	L	L	L
0.880	L	L	L	L	*	*	L	L	L	L	L	L	L	L	L	L	L	L	L	L	L	L	L	L	L	L	L	L	L	L	L
0.890	L	L	L	L	*	L	L	L	L	L	L	L	L	L	L	L	L	L	L	L	X										
0.900	L	L	L	*	L	L	L	L	L	L	L	0	L	L	L	L	L	L	L	-											
0.910	L	L	*	*	L	L	L	L	L	L	L	0	L	L	L	L	L	L	L	-											
0.920	L	L	*	L	L	L	L	L	L	L	L	0	L	L	L	L	L	L	-	-											
0.930	L	*	L	L	L	L	L	L	L	L	L	0	L	L	L	L	L	L	-												
0.940	L	*	L	L	L	L	L	L	L	L	L	L	L	L	L	L	L	L	-												
0.950	*	L	L	L	L	L	L	L	L	L	L	L	0	L	L	L	L	-													
0.960	*	L	L	L	L	L	L	L	L	L	L	L	0	L	L	L	L	-													
0.970	L	L	L	L	L	L	L	L	L	L	L	L	0	L	L	L	-														
0.980	L	L	L	L	L	L	L	L	L	L	L	L	0	L	L	L	-														
0.990	L	L	L	L	L	L	L	L	L	L	L	L	0	L	L	-															
1.000	L	L	L	L	L	L	L	L	L	L	L	L	0	L	L	-															
1.010	L	L	L	L	L	L	L	L	L	L	L	L	0	L	-	-															
1.020	L	L	L	L	L	L	L	L	L	L	L	L	0	L	-																
1.030	L	L	L	L	L	L	L	L	L	L	L	L	0	-	-																
1.040	L	L	L	L	L	L	L	L	L	L	L	0	0	-																	
1.050	L	L	L	L	L	L	L	L	L	L	L	0	-	-																	
1.060	L	L	L	L	L	L	L	L	L	L	L	0	-																		
1.070	L	L	L	L	L	L	L	L	L	L	0	-	-																		
1.080	L	L	L	L	L	L	L	L	L	L	0	-																			
1.090	L	L	L	L	L	L	L	L	L	0	-	-																			
1.100	L	L	L	L	L	L	L	L	L	0	-																				
1.110	L	L	L	L	L	L	L	L	0	-	-																				
1.120	L	L	L	L	L	L	L	0	0	-																					
1.130	L	L	L	L	L	L	0	0	-																						
1.140	L	L	L	L	0	0	L	L	-																						
1.150	L	L	L	0	0	L	L	-																							

Figure 5.6 Going to Hexagonal Closest Packing.

In this case, the unconstrained solution goes beyond mechanical limits and off the top of the zone of variations. However, the circle of signs indicates a local minimum at H_2, which is marked by an X. This is an example of case 2 as shown in Figure 5.3.

6. Optimization with Energy or Power Constraints

An optimization study may seek to determine the optimum scale of a system, or it may provide a constraint on the system size. For central receiver systems the most natural constraint is the total thermal power at the design time. The optimization described in section 2 is unconstrained. Our first look at the effect of constraints will be for fixed annual energy. We assume a specific tower height, receiver size, and cost.

Given the figure of merit

$$F = C/E,$$

with

$$C = C_o + C_h A_G$$

$$A_G = \sum_c A_c = \bar{A}\sum_c f_c \phi_c$$

and

$$E = a\bar{S}\sum_c \eta_c \lambda_c A_c - b = a\bar{A}\bar{S}\sum_c \eta_c \lambda_c f_c \phi_c - b.$$

We need MIN(F) with $E = \bar{E}$ (i.e., $\bar{E}$ is given). Clearly,

$$\text{MIN}(F) = \text{MIN}\{C \mid E = \bar{E}\}/\bar{E}$$

The standard Lagrangian technique can be used for finding the minimum under constraints. Let

$$g = E/(\bar{S}\bar{A}) = a\sum_c \eta_c \lambda_c f_c \phi_c - b/(\bar{S}\bar{A})$$

and

$$h = C/(C_h\bar{A}) = C_o/(C_h\bar{A}) + \sum_c f_c \phi_c.$$

In this case g is the constraint. Consequently,

$$\text{MIN}(F) = C_h\bar{A}\ \text{MIN}(h)/\bar{E}$$

when

$$\partial_{f_c} g - L\partial_{f_c} h = 0 \qquad \text{(Eq. 6.1)}$$

$$\partial_{t_c} g - L\partial_{t_c} h = 0 \qquad \text{(Eq. 6.2)}$$

and

$$\partial_{\phi_c} g - L\partial_{\phi_c} h = 0 \qquad \text{(Eq. 6.3)}$$

For internal cells $\phi_c=1$, and equation (6.1) gives

$$a\eta_c(\lambda_c+f_c\partial_{f_c}\lambda_c) - L\cdot 1 = 0,$$

which can be solved for the Lagrangian parameter L.

$$L = a\eta_c(\lambda_c+f_c\partial_{f_c}\lambda_c)$$

Equation (6.2) gives

$$a\eta_c(\partial_{t_c}\lambda_c)f_c - L\cdot 0 = 0,$$

or, equivalently,

$$\partial_{t_c}\lambda_c = 0.$$

Similarly, equation (6.3) gives

$$a\eta_c\lambda_c f_c - Lf_c = 0,$$

so that

$$B_c \equiv a\eta_c\lambda_c/L \geq 1$$

for cells inside the trim line.

Notice that L replaces $\tilde{\mu}$ as the cell matching parameter, and the two optimum cell conditions remain unchanged. The boundary condition also appears unchanged, and the Lagrangian parameter L is determined by the constraint

$$\bar{E} = E(L) = a\bar{S}\bar{A}\sum_c{}^{*}\eta_c\lambda_c f_c - b.$$

Σ^* denotes a summation over those cells for which $L \leq a\eta_c\lambda_c$.

Although the input value of F is not mentioned in the above derivation, it is convenient to assume that

$$L_{IN} = C_h/(F(\text{input})a\bar{S}),$$

so that L_{IN} is proportional to the input figure of merit F(input). After several trials, F(output)$\twoheadrightarrow$F(input) and

$$\bar{E} = E(L_{IN})$$

as required.

The fixed power constraint requires another sum over cells to represent the available thermal power at design time. Let P_o represent the available thermal power at time τ_o when the direct beam insolation at normal incidence is σ_0. ξ_c gives the efficiency for redirected power from cell c at time τ_o. As in section 2.3

$$P = a\sigma_o\bar{A}\Sigma\eta_c\xi_c f_c\phi_c - b/\bar{H}$$

For simplicity, let

$$C = C_o + C_h\,\bar{A}\,(\sum_c f_c\phi_c)$$

and F = C/E, as always. The fixed power optimization requires

$$F = \text{Min}\,\{F(V) \mid P = P_o\}.$$

Equations (6.1-6.3) apply, with

$$g = P, \text{ and } h = F.$$

Hence, the equations for a constrained optimum are of the form

$$\partial P - L\partial F = 0 \qquad \text{or} \qquad \partial F = \partial P/L$$

with $\partial = \partial_{f_c}, \partial_{t_c}$, and ∂_{ϕ_c}. As always, ∂F is

$$\partial F = \partial C/E - C\,\partial E/E^2$$

so that

$$\partial C - F\,\partial E - (E/L)\,\partial P = 0.$$

Equation 6.1 gives

$$C_h\bar{A} - Fa\bar{S}\bar{A}\eta_c(\lambda_c+f_c\partial_{f_c}\lambda_c) - (E/L)a\sigma_o\bar{A}\eta_c(\xi_c+f_c\partial_{f_c}\xi_c) = 0,$$

or, equivalently,

$$\tilde{\mu} = \mu_c(f_c,t_c) + (E\sigma_o/(LF\bar{S}))\,\upsilon_c(f_c,t_c) = C_h/(Fa\bar{S})$$

where

$$\mu_c = \eta_c\,(\lambda_c+f_c\,\partial_{f_c}\lambda_c),$$

and

$$\upsilon_c = \eta_c\,(\xi_c+f_c\,\partial_{f_c}\xi_c).$$

Equation 6.2 gives

$$-Fa\bar{S}\bar{A}\eta_c f_c\partial_t\lambda_c - (E/L)a\sigma_o\bar{A}\eta_c f_c\partial_{t_c}\xi_c = 0$$

so that

$$\partial_{t_c}\lambda_c = (E\sigma_o/(LF\bar{S}))\,\partial_{t_c}\xi_c \neq 0.$$

Equation 6.3 gives

$$C_h\bar{A}f_c - Fa\bar{S}\bar{A}\eta_c\lambda_c f_c - (E/L)a\sigma_0\bar{A}\eta_c\xi_c f_c = 0$$

so that for a boundary cell

$$\tilde{\mu} - \eta_c\lambda_c - (E\sigma_o/(LF\bar{S}))\,\eta_c\xi_c = 0 \quad .$$

$\eta_c\lambda_c$ is larger for interior cells than for boundary cells, hence, for interior cells

$$\tilde{\mu}/(\eta_c\lambda_c) \leq 1 + (E\sigma_o/LF\bar{S}))\ \xi_c/\lambda_c\ .$$

L must be determined by the constraint

$$P_0 = P(L) = a\sigma_0\bar{A} \sum_c \eta_c\xi_c f_c\phi_c(L) - b/\bar{H}.$$

This type of optimization has not been implemented because of the difficulty of solving for L.

As in Section 2.3, it convenient to assume that

$$E_{inc} = H_o\ P_{inc}, \qquad \text{(Eq. 6.4)}$$

so that

$$\partial P = \partial E/H_o\ ,$$

and in this case the equations of the constrained optimum require

$$\partial C = (F+E/(LH_o))\ \partial E.$$

Equations 6.1-6.3 become

$$\tilde{\mu} = (1+E/(FLH_o))\mu_c(f_c,t_c)$$

$$\partial_t\lambda_c = 0,$$

and

$$B_c = (1+E/(FLH_o))\eta_c\lambda_c/\tilde{\mu} \geq 1$$

for interior cells. L satisfies $P_o = P(L)$. These optimum conditions are equivalent to the unconstrained equations if

$$\tilde{\mu}\rightarrow\rightarrow\mu^* = C_h/(F^*a\bar{S})$$

$$= \tilde{\mu}(1+E/(FLH_o))^{-1}.$$

Consequently,

$$F^* = F+E/(LH_o) = F(\text{input})$$

and

$$L = (F^*-F)H_o/E.$$

This solution is obtained by varying the F(input) until $P_o = P$.

7. Simultaneous Optimization of the Collector and Receiver Geometry

Let $F = C/E$ be the figure of merit; however, we will now extend the set of independent variables to include h for the height (vertical length), of the receiver, r for the radius of the receiver, and T for the focal height of the tower. Let

$$V = \{r,h,T,(R_c,Z_c,\phi_c) \quad c \;\varepsilon\; \text{field}\}$$

be the extended set. $\{(R_c,Z_c,\phi_c)\}$ represents the collector field.

In this section the cost model will include the receiver and the tower. Let

$$C = C_o + C_r A_r + C(T,P) + C_h \bar{A} \sum_c \phi_c \psi_c$$

where

C_o = fixed cost for balance of system,

C_r = cost of receiver per unit area,

$A_r = 2\pi\, rh$ = area of receiver,

$C(T,P)$ = cost of tower as a function of tower height T and power P at design time τ_o, and

ψ_c includes the cost of heliostats, land, and wiring as in section 2.

E is the total annual thermal energy available at the base of the tower in an average year.

$$E = a\, \bar{S}\bar{A}\, (\sum_c \eta_c \lambda_c f_c \phi_c) - b$$

with

$$a = \hat{\alpha}\hat{\rho} = (\text{absorptivity})\ (\text{reflectivity})\ (\text{etc.}),$$

and

$$b = \bar{H}\, A_r P_r(t_o)$$

where $\bar{H}$ is the number of hours per year of useful insolation (i.e. receiver operation), $P_r(t_o)$ is the radiative and convective loss rate from the receiver per unit area, and t_o is the operating temperature of the receiver. $P_r(t_o)$ is assumed to be known.

We will not discuss the optimization with respect to operating temperature because our figure of merit is unsuitable and the necessary cost information is unavailable. The solution is well known, assuming Carnot efficiency and no temperature dependent costs. Another approach to the receiver loss problem has been developed. (See Reference 20, 21, 22).

In this section, we assume an unconstrained optimization. Therefore, the solution for the collector geometry is formally the same as in section 2 with

$$C_o \twoheadrightarrow C_o + C_r A_r + C(T,P)$$

and for given values of (h,r,T).

The receiver geometry problem requires three additional optimum conditions for reciever height, reciever radius, and tower height.

$$\delta_h F = 0 = \delta_r F = \delta_T F,$$

or, equivalently,

$$\partial_h E/\partial_h C = 1/F, \text{ etc.}$$

For convenience, let

$$\Lambda = \sum_c \eta_c \lambda_c f_c \phi_c .$$

It is easy to see that

$$\partial_h C = C_r A_r / h$$

$$\partial_r C = C_r A_r / r$$

$$\partial_T C = \partial_T C_T$$

$$\partial_h E = a\bar{S}\bar{A}\partial_h \Lambda - \bar{H} A_r P_r / h$$

$$\partial_r E = a\bar{S}\bar{A}\partial_r \Lambda - \bar{H}A_r P_r / r$$

and

$$\partial_T E = a\bar{S}\bar{A}\partial_T \Lambda .$$

Consequently,

$$h\partial_h \Lambda = A/B + 1/BF \qquad \text{(Eq. 7.1)}$$

$$r\partial_r \Lambda = A/B + 1/BF \qquad \text{(Eq. 7.2)}$$

where

$$A = \bar{H}P_o/C_r ,$$

and

$$B = a\bar{S}\bar{A}/C_r A_r$$

Similarly,

$$a\bar{S}\bar{A}\partial_T \Lambda / \partial_T C_T = 1/F ,$$

and, therefore, (after applying a factor of T and some re-arrangement)

$$T\partial_T \Lambda = T\partial_T C_T/(a\bar{S}\bar{A}F) \qquad \text{(Eq. 7.3)}$$

$$\cong 2C_T/(a\bar{S}\bar{A}F)$$

for tower cost quadratic in T. Equations 7.1, 7.2, and 7.3 are difficult to solve, and it is necessary to know the cooresponding partial derivatives of η_c (i.e., $\partial_h \eta_c$, $\partial_r \eta_c$, and $\partial_T \eta_c$).

Consequently, we propose to seek the minimum value of F(r,h), which is consistent with the trim boundary and total power, by direct numerical methods rather than by the optimum requirements $\delta_h F = 0$ and $\delta_r F = 0$.

Given the nodal interception data $\eta_{cpq}(r,h)$ for a receiver of size (r,h), we can construct the interception fractions for receivers of various sizes. The receiver nodes {(p,q)} correspond to receiver heights h_q for q=1 ... Q and receiver azimuths ϕ_p for p=1 ... P. All of these nodes have radius $\bar{r}$.

We have

$$h_q = q\Delta h,$$

and

$$\phi_p = p\ \Delta\phi$$

where

$$\Delta h = \bar{h}/Q,$$

and

$$\Delta\phi = 2\pi/P.$$

The greatest interception is obtained by summing all of the nodes

$$\eta_c(\bar{r},\bar{h}) = \sum_{p=1}^{P} \sum_{q=1}^{Q} \eta_{cpq}\ .$$

However, shorter cylinders are easily represented by omitting a few rings of nodes at the top and the bottom of the cylinder:

$$\eta_c(\bar{r},h_\beta) = \sum_{p=1}^{P} \sum_{q=\beta}^{Q-\beta} \eta_{cpq}$$

where

$$h_\beta = \beta\Delta h.$$

Cylinders of smaller radius are more difficult to represent. However, the task can be accomplished by interpolating panel interception fractions. Let

$$\eta_{cp}(h_\beta) = \sum_{q=\beta}^{Q-\beta} \eta_{cpq}$$

represent the panel interception factor for the p-th panel with a height h_β. The center of the p-th panel has the azimuth angle

$$\phi_p = (p+\tfrac{1}{2})\,\Delta\phi$$

measured east from south (i.e. counterclockwise). The edges of the panel have the azimuths p $\Delta\phi$ and $(p+1)\,\Delta\phi$. If cell c has azimuth ϕ_c, the perpendicular distance from the edge of the panel to the center line from cell c is given by

$$D_{cp\pm} = \bar{r} \sin (\phi_c - \phi_p \pm \tfrac{1}{2}\Delta\phi).$$

Let

$$D_{cp} = \text{MAX } D_{cp\pm} \,,$$

and let

$$E_{p_1 p_2} = \sum_{p=p_1}^{p_2} \eta_{cp}(h_\beta)$$

so that the interpolated interception fraction is given by

$$\eta_c(r_\alpha,h_\beta) = E_{p_1 p_2} + f_1\eta_{c(p_1-1)} + f_2\eta_{c(p_1+1)}$$

for the appropriate values of p_1, p_2, f_1, and f_2. (See Figure 7.1). f_1 and f_2 are suitable fractions of unity to represent a cylinder of radius r_α.

The subroutine RCFINT can be generalized to construct the interception $\eta_c(r_\alpha,h_\beta)$ for any

$$r_\alpha \leqq \bar{r} \text{ and } h_\beta \leqq \bar{h}$$

in terms of the nodal interception data obtained from a cylindrical receiver of radius $\bar{r}$ and height $\bar{h}$. It is then feasible to explore the dependence of the output figure of merit on (r_α,h_β). Interception due to a flat plate receiver depends on its length, width, and orientation. If the optimum orientation can be assumed, then the two variable optimization over length and width is similar to the cylindrical case. (See Figure 7.2 and 7.3).

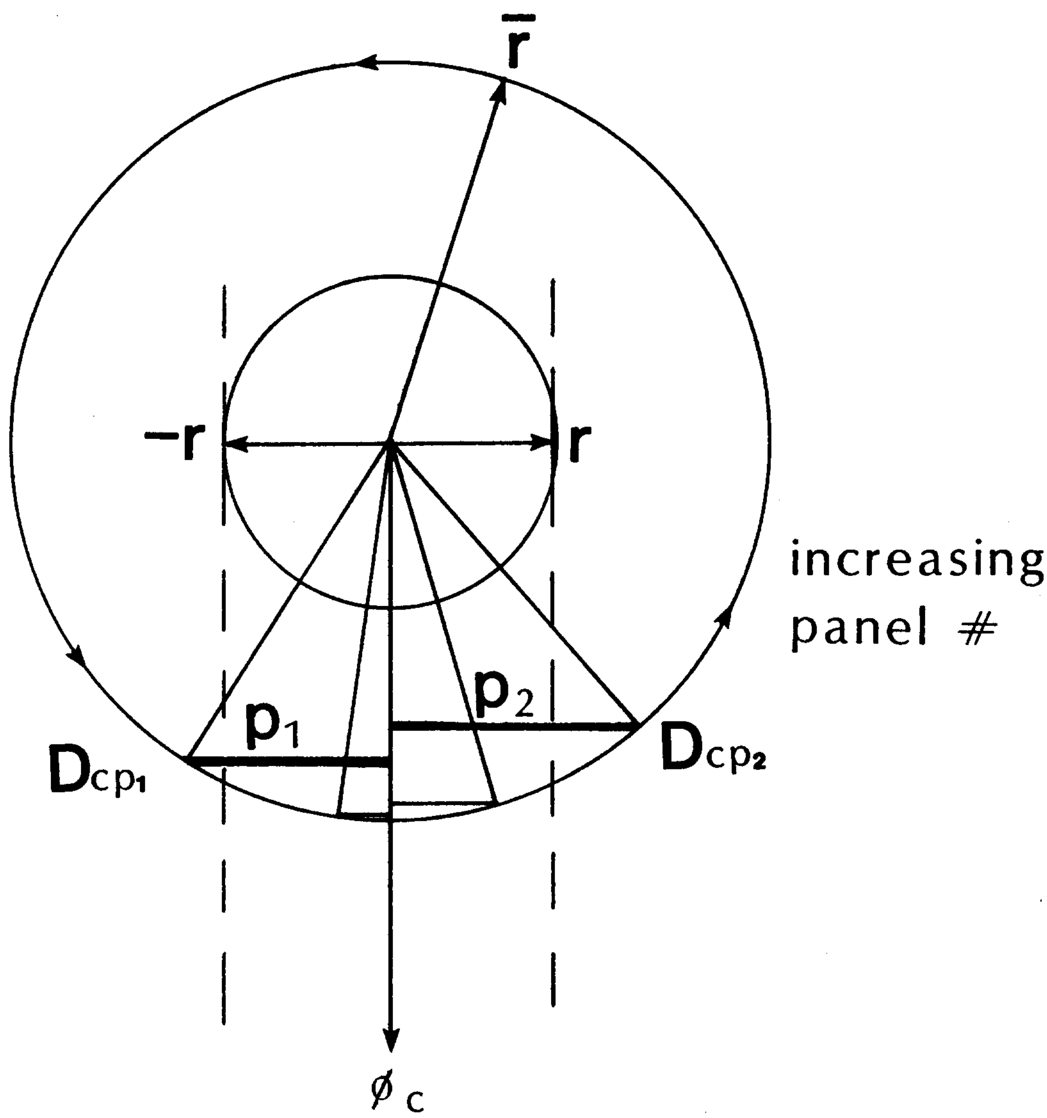

Figure 7.1 Panel Panel Interpolation for Smaller Cylinders.

ϕ_c points towards the center of cell c. p_1 is the first panel such that $D_{cp_1} \geq r$, and p_2 is the last panel such that $D_{cp_2} \geq r$. The panels in the set $(p_1 \ldots p_2)$ provide the same interception as all of the panels in the smaller cylinder (if the end corrections f_1 and f_2 are included).

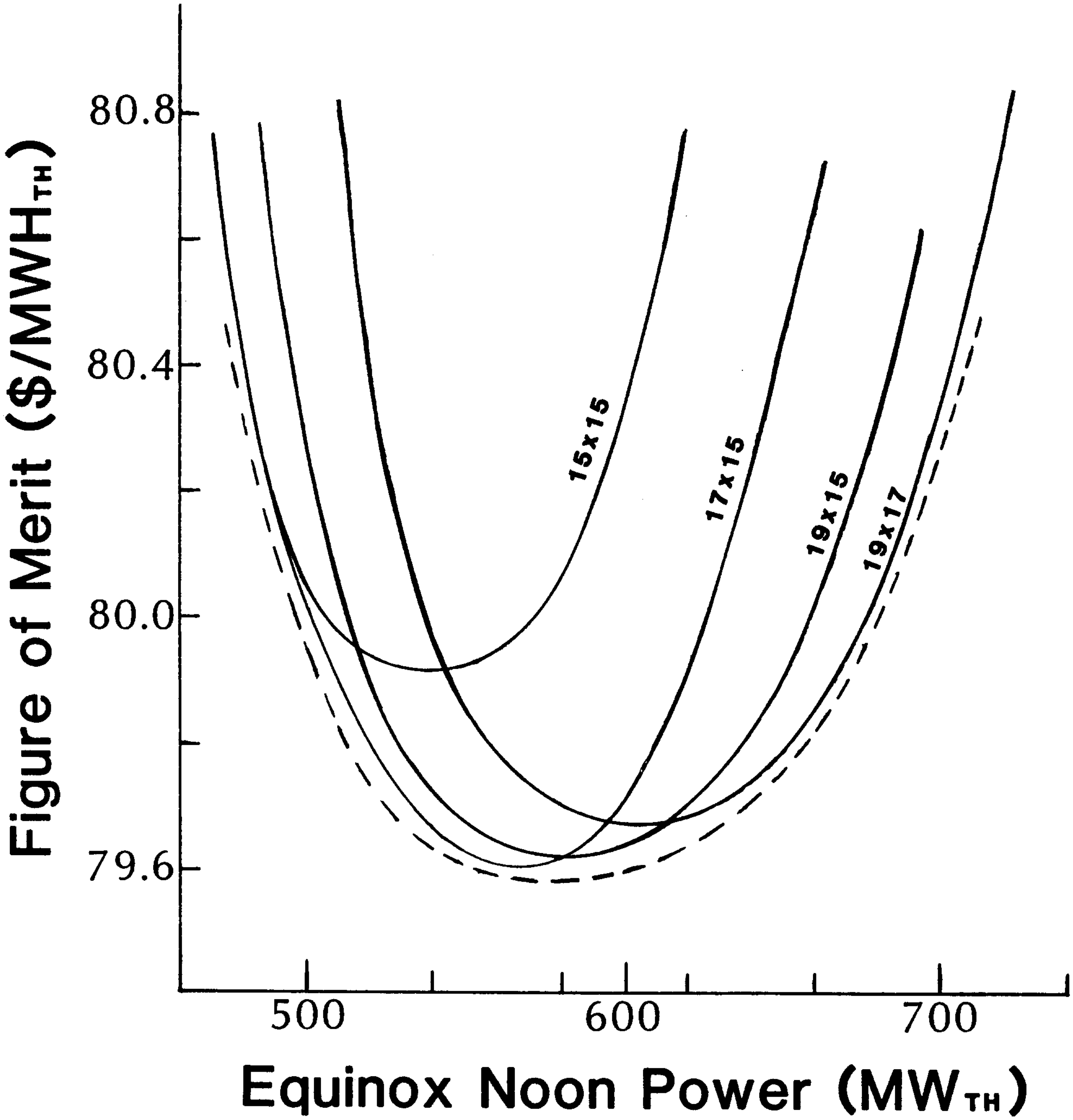

Figure 7.2 Figure of Merit for Various Receiver Sizes.

Each solid curve represents the specified receiver size. The parabolic curves are obtained by varying the input figure of merit. The dotted curve is the envelope of the parabolic curves for given tower height at various noon powers.

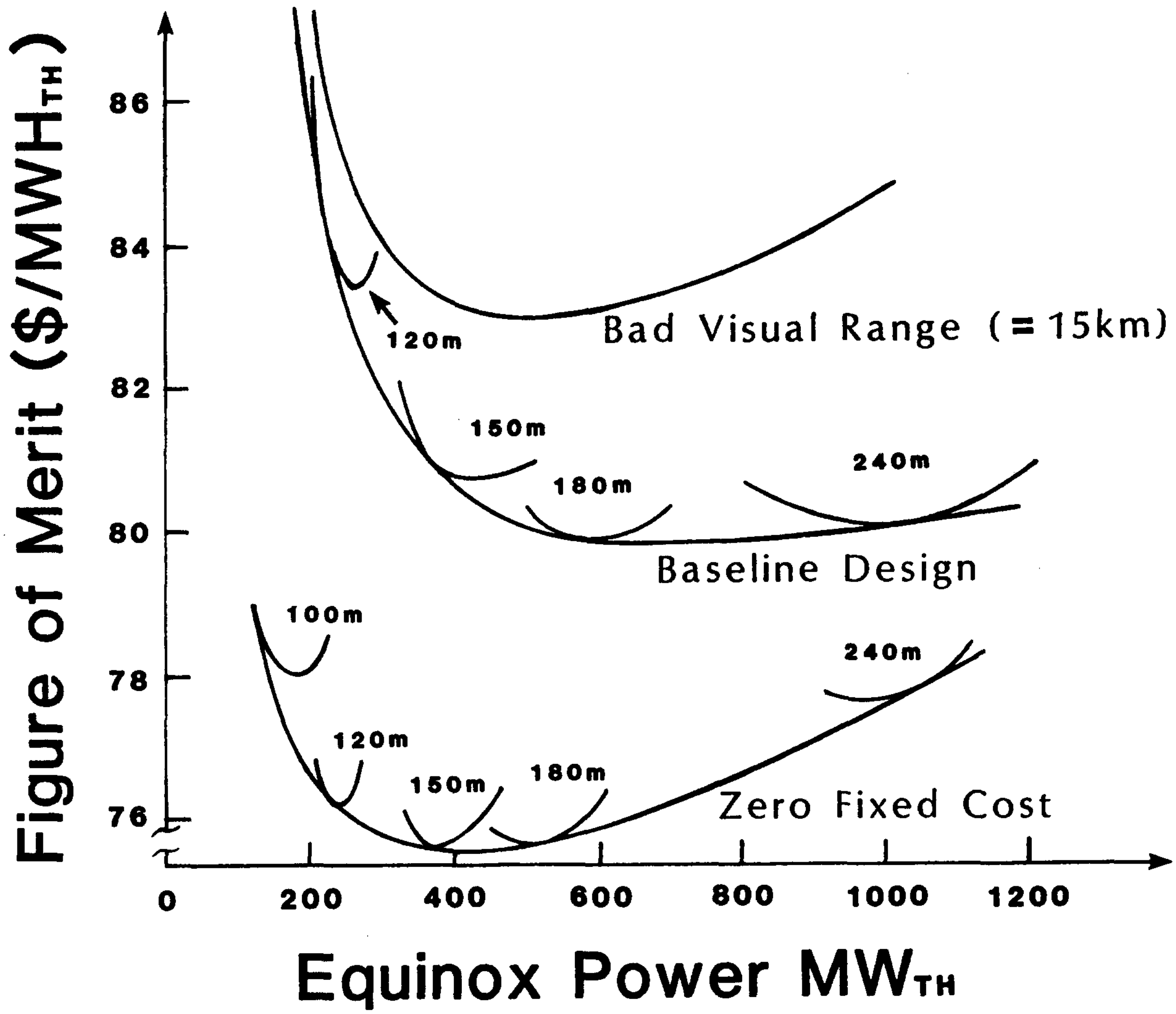

Figure 7.3 Figure of Merit for Various Tower Heights.

Each inlaid curve represents an envelope of optima as shown in the previous figure. The envelope of tower height optima provides the grand optimum versus noon power. Three different models are shown to indicate the effect of fixed cost and visual range. The baseline visual range is 50 km and fixed cost is $2.6 M.

8. References

(1) A New Method for Collector Field Optimization, M. S. Abdel-Monem, A. F. Hildebrandt, F. W. Lipps, and L. L. Vant-Hull, Heliotechnique and Development, 1 pp. 372-387 (1976). Available from Development Analysis Associates, Inc., 675 Mass. Ave, Cambridge, Mass 02139. See Proceedings of the Comples International Conference, Dhahran, Saudi Arabia, Nov. 2-6, 1975.

(2) Proceedings of the ERDA Solar Workshop on Methods for Optical Analysis of Central Receiver Systems organized by the University of Houston Solar Energy Laboratory for SANDIA Laboratories, Livermore, under ERDA Contract AT(29-1)-789, August 10-11, 1977. Available from NTIS. See the following articles:

a) M. D. Walzel, Image Generation for Solar Central Receiver Systems, p. 39-60.

b) F. W. Lipps, The Receiver Programs, p. 61-66.

c) F. W. Lipps, The Shading and Blocking Processor, p. 67-75.

c) F. W. Lipps, Collector Field Optimization and Layout, p. 249-272.

(3) A Cellwise Method for the Optimization of Large Central Receiver Systems, F. W. Lipps and L. L. Vant-Hull, Journal of Solar Energy 20 pp. 505-516. (1978).

(4) Solar Central Receiver Heliostat Field Analysis: 1) Slope and Latitude study, 2) Net Energy Analysis, 3) Locating the Sun, 4) the Sodium Heat Engine; Final Report - Part II, prepared by the Energy Laboratory, University of Houston under ERDA Grant No. EG-76-G-05-5178. May 1978, ORO 5178-78-2-UC62.

(5) Parametric Study of Optimzed Central Receiver Systems, F. W. Lipps and L. L. Vant-Hull, Proceedings of the 1978 Annual Meeting of American Section of ISES at Denver, Colorado, Vol 1, pp. 793-798.

(6) Technical Memo: Notes on Collector Field Optimization, F. W. Lipps and L. L. Vant-Hull, to internal distribution (manuscript date November 15, 1978). Present document supercedes this technical memo.

(7) 10 MWe Solar Thermal Central Receiver Pilot Plant, Solar Facilities Design Integration, Collector Field Layout Specification (RADL ITEM 2-12), Sept. 1979 under contract DE-AC03-79SF-10499, See SAN/0499-18 or MDC-G8201. Also Collector Field Optimization report (RALD 2-25) Jan 1981, SAN/0499-22 MDC G8214.

(8) An Investigation of Optimum Heliostat Spacings for the Sub-Tower Region of a Solar Power Plant, M. D. Walzel, SUN II, Proceedings of the International Solar Energy Society, Silver Jubilee Congress. Atlanta, Georgia - May, 1979, Vol. 2, p. 1243.

(9) Simulation and Design Methods for a Solar Central Receiver Hybrid Power System, M. D. Walzel, Proceedings of Systems Simulation and Economic Analysis Conference, Jan. 23, 1980, San Diego, California.

(10) Optimization of Heliostat Fields for Solar Tower Systems," L. L. Vant-Hull, Solar Power Systems, Colloques Internationaux Du Centre National de la Recherche Scientique No. 306, Marseille, June 15-20, 1980, STS-80-47, p. 319.

(11) A Programmer's Manual for the University of Houston Computer Code, RCELL, F. W. Lipps and L. L. Vant-Hull, Sept., 1980, SAN/0763-1.

(12) A User's Manual for the University of Houston Computer Code - RC: Cellwise Optimization, C. L. Laurence and F. W. Lipps, December, 1980, SAN/0763-3.

(13) A User's Manual for the University of Houston Solar Central Receiver - Cellwise Performance Model: NS (Volumes 1 and 2), F. W. Lipps and L. L. Vant-Hull, December, 1980, SAN/0763-4.

(14) 5th Quarterly Progress Report on Contract AC03-79-SF19769, L. L. Vant-Hull, January 10, 1981.

(15) Programmer's Manual for CREAM: Cavity Radiation Exchange Analysis Model, F. W. Lipps, February, 1981, University of Houston Energy Laboratory.

(16) Theory of Cellwise Optimization for Solar Central Receiver Systems, F. W. Lipps, September, 1981, SAN/7637-1.

(17) User's Manual for the University of Houston Individual Heliostat Layout and Performance Code, C. L. Laurence and F. W. Lipps, April, 1982, SANDIA Procurement 84-1637.

(18) Generalized Layout for Collector Field with Broken Planes Including Modifications to the RC-Optimization, CELLAY, and IH-Performance Codes, F. W. Lipps, December 1982, SANDIA Procurement 84-1637.

(19) Cavity Design Capability and Incident Flux Density Code, F. W. Lipps, March, 1983. Submitted for review to SERI.

(20) Computer Simulation of Shading and Blocking Discussion of Accuracy and Recommendations by F. W. Lipps, Dec. 1, 1983. (In review by SERI).

(21) "Effect of High Receiver Thermal Loss Per Unit Area on The Performance of Solar Central Receiver Systems Having Optimum Heliostat Fields and Optimum Receiver Aperture Areas" by Charles L. Pitman. PhD. Dissertation, December, 1983.

(22) Receiver Loss Study: Optics of High Temperature Solar Central Receiver Systems by C. L. Pitman and L. L. Vant-Hull, Dec., 1981. (In review by SNLL.)

(23) "Effect of High Receiver Thermal Loss on the Efficiency of Central Receiver Systems Having Optimum Heliostat Fields and Optimum Receiver Aperture Areas", by C. L. Pitman and L. L. Vant-Hull, Proceedings of Solar Thermal Research Workshop in Sept. 1983, Georgia Institute of Technology (Atlanta, Nov. 1983); also Proceedings of the International Seminar on Solar Thermal Heat Production and Solar Fuels and Chemicals (Stuttgart FRG, Oct. 1983).

(24) Atmospheric Transmittance Model for a Solar Beam Propagating Between a Heliostat and a Receiver, C. L. Pitman and L. L. Vant-Hull, SAND 83-8177; SNLL, NTIS A05.

UNLIMITED RELEASE
INITIAL DISTRIBUTION

U.S Department of Energy (5)
Forrestal Building
1000 Independence Avenue, S.W.
Washington, D.C. 20585
Attn: H. Coleman
C. Carwile
C. Mangold
F. Morse
M. Scheve

U.S. Department of Energy (2)
1333 Broadway
Oakland, CA 94612
Attn: R. W. Hughey
T. Veath

U. S. Department of Energy (2)
Albuquerque Operations Office
P.O. Box 5800
Albuquerque, NM 87115
Attn: J. Weisiger
D. Graves

University of California (2)
Mechanical Engineering Dept.
Berkeley, CA 94720
Attn: J. A. C. Humphrey
R. Greif

University of Houston (32)
Solar Energy Laboratory
4800 Calhoun
Houston, TX 77004
Attn: A. F. Hildebrandt
F. W. Lipps
C. L. Pitman (5)
L. L. Vant-Hull (25)

University of Illinois
1206 W. Green Street
Urbana, IL 61820
Attn: A. M. Clausing

Washington State University
Dept. of Mechanical Engineering
Pullman, WA 99164-2920
Attn: C. Crowe

Aerospace Corporation, The
Solar Thermal Projects
Energy Systems Group
P. O. Box 92957
Los Angeles, CA 90009
Attn: P. Munjal

Arco Power Systems
7061 S. University, Suite 300
Littleton, CO 80122
Attn: F. A. Blake

Arco Power Systems
302 Nichols Drive
Hutchins, TX 75141
Attn: R. L. Henry

Arizona Public Service Company
P.O. Box 21666
Phoenix, AZ 85036
Attn: E. Weber

Babcock and Wilcox
91 Stirling Avenue
Barberton, OH 44203
Attn: G. Grant

Badger Energy, Inc.
One Broadway
Cambridge, MA 02142
Attn: C. A. Bolthrunis

Battelle Pacific Northwest Laboratories
P.O. Box 999
Richland, WA 99352
Attn: T. A. Williams

Bechtel Group, Inc.
P.O. Box 3965
San Francisco, CA 94119
Attn: Pascal DeLaquil

Black and Veatch Consulting Engineers (2)
P.O. Box 8405
Kansas City, MO 64114
Attn: J. C. Grosskreutz
J. E. Harder

Boeing Aerospace Company
Energy Systems
P.O. Box 3999, MS87-63
Seattle, WA 98124
Attn: W. D. Beverly

El Paso Electric Company
P. O. Box 10412
El Paso, TX 79946
Attn. J. E. Brown

Electric Power Research Institute
P.O. Box 10412
Palo Alto, CA 94303
Attn: E. DeMeo

Energy Systems Group (2)
Rockwell International
8900 DeSoto Ave.
Canoga Park, CA 91304
Attn: T. Springer
A. Ullman

Foster Wheeler Development Corporation (3)
12 Peach Tree Hill Road
Livingston, NJ 07039
Attn: G. Carli
S. Goidich
R. J. Zoschak

Garrett AiResearch Mfg. Co.
2525 W. 190th Street
Torrance, CA 90509
Attn: M. Combs

G. A. Technologies (2)
P. O. Box 85608
San Diego, CA 92138
Attn: G. Besenbruch
L. Brown

Georgia Institute of Technology (2)
Solar Energy & Materials Tech. Div.
Engineering Experiment Station
Atlanta, GA 30332
Attn: R. A. Cassanova

Gibbs and Hill, Inc.
393 Seventh Avenue
New York, NY 10001
Attn: R. Prieto

Lawrence Berkeley Laboratory
University of California
Berkeley, CA 94720
Attn: A. J. Hunt

Los Angeles Department of Water and Power
111 North Hope St.
Los Angeles, CA 90051
Attn: D. Chu

McDonnell Douglas Astronautics Company
5301 Bolsa Avenue
Huntington Beach, CA 92647
Attn: R. L. Gervais

North Carolina State Univ.
Chemical Engineering Dept.
P. O. Box 7905
Raleigh, NC 27695
Attn: Prof. R. Carbonell

Olin Chemical Company
120 Long Ridge Road
Stamford, CT 06904
Attn: L. C. Firouccio

Olin Chemicals Group
P. O. Box 2896
Lake Charles, LA 70624
Attn: J. Morgan

Pacific Gas and Electric Company
3400 Crow Canyon Road
San Ramon, CA 94526
Attn: G. Braun

Pacific Northwest Laboratory
P. O. Box 999
Richland, WA 99352
Attn: K. Drost

The Ralph M. Parsons Company
100 West St.
Pasadena, CA 91124
Attn: N. W. Snyder

PFR Energy Systems, Inc.
P. O. Box 91890
Los Angeles, CA 90045
Attn: T. Rosenman

Polydyne, Inc.
1900 S. Norfolk St., Suite 209
San Mateo, CA 94403
Attn: P. B. Bos

Public Service of New Mexico
P. O. Box 2267
Albuquerque, NM 87103
Attn: A. Akhil

Rockwell International
Energy Systems Group
8900 De Soto Avenue
Canoga Park, CA 91304
Attn: T. Springer

Rockwell International (2)
Rocketdyne Division
6633 Canoga Avenue
Canoga Park, CA 91304
Attn: J. M. Friefeld
R. Surette

San Diego Gas and Electric Company
Mechanical Engineering
P.O. Box 1831
San Diego, CA 92112
Attn: R. E. Potthoff

Solar Energy Industries Association
1140 19th St., N.W.
Suite 600
Washington, D.C. 20036
Attn: C. LaPorta

Solar Energy Research Institute (7)
1617 Cole Boulevard
Golden, CO 80401
Attn: J. Anderson
R. J. Copeland
B. Gupta
D. Johnson
M. Murphy
G. Nix
J. Thornton

Solar Power Engineering Co.
P. O. Box 91
Morrison, CO 80465
Attn: H. C. Wroton

Southern California Edison
Solar One Project
P. O. Box 411
Daggett, CA 92327
Attn: C. Lopez

Southern California Edison (2)
P.O. Box 800
Rosemead, CA 92807
Attn: J. N. Reeves
P. Skvarna

Spectra Technology, Inc.
2755 Northrup Way
Bellevue, WA 98004
Attn: R. R. Taussig

Stearns Catalytic Corp.
P.O. Box 5888
Denver, CO 80217
Attn: W. R. Lang

University of California
Lawrence Livermore Natl. Lab.
Livermore, CA 94550
Attn: O. Walton, L-200

E. H. Beckner, 6000; Attn: V. Dugan, 6200
D. G. Schueler, 6220; Attn: J. V. Otts, 6222
J. A. Leonard, 6227

R. S. Claassen, 8000; Attn: D. M. Olson, 8100
A. N. Blackwell, 8200
D. L. Hartley, 8300
C. S. Selvage, 8000A
C. W. Robinson, 8240; Attn: C. Hartwig, 8244
R. J. Kee, 8245
G. H. Evans, 8245
W. G. Houf, 8245
C. A. LaJeunesse, 8245
W. Winters, 8245

R. C. Wayne, 8400; Attn: L. D. Bertholf, 8430
H. Hanser, 8440
R. L. Rinne, 8470
P. K. Falcone, 8471
A. C. Skinrood, 8471
D. B. Dawson, 8473
J. M. Hruby, 8473
C. L. Mavis, 8473
J. C. Swearengen, 8473 (15)
J. J. Iannucci, 8475

M. E. John, 8478
Publications Division 8265, for TIC (30)
Publications Division 8265/Technical Library Processes Division, 3141
Technical Library Processes Division, 3141 (3)
M. A. Pound, 8024, for Central Technical Files (3)